

REPORT**Clinical behaviour of spinocerebellar ataxia type 12 and intermediate length abnormal CAG repeats in *PPP2R2B*****Achal K. Srivastava,^{1,*} Amit Takkar,¹ Ajay Garg² and Mohammed Faruq^{3,*}**

*These authors contributed equally to this work.

Spinocerebellar ataxia type 12 (SCA12) is a rare neurodegenerative disorder caused by CAG repeat expansion in the *PPP2R2B* gene. Previously, the causal length of CAG repeats ascribed to SCA12 was more than 51; however, a few reports have also described unusual occurrence of CAG repeat length 36–51 repeats among patients of different geographical population, with atypical clinical association. From our systematic search for SCA12 in a genetic screening programme, we have identified a large number of SCA12 cases. In this study, we specifically describe the clinical behaviour of 18 patients who harbour CAG repeats in the range of 43–50 and compare their clinical behaviour with patients carrying typical pathogenic threshold length of 51 CAG repeats. Unsurprisingly, we observed that the clinical characteristics were similar to those of typical SCA12 phenotype, with large variability in the age at onset. Radiologically, we observed a variable degree of cerebro-cerebellar degeneration along with white matter changes that do not correlate with the disease severity. We define a new pathogenic threshold of CAG-43 to be pathogenic for SCA12 diagnosis and also describe the clinical profiles of two biallelic CAG expansion carriers. We also propose that SCA12 might not be that restricted in terms of occurrence in other geographical or ethnic populations, as it was previously presumed to be.

1 Neurology Department, Neuroscience Centre, All India Institute of Medical Sciences, New Delhi, India

2 Neuroradiology Department, Neuroscience Centre, All India Institute of Medical Sciences, New Delhi, India

3 Genomics and Molecular Medicine, CSIR-Institute of Genomics and Integrative Biology (CSIR -IGIB), Mall Road, Delhi 110007, India

Correspondence to: Dr Achal Kumar Srivastava, MD, DM,
Professor, Department of Neurology,
Neuroscience centre, All India Institute of Medical Sciences,
Ansari Nagar, New Delhi, India
E-mail: achalsrivastava@hotmail.com

Correspondence may also be addressed to: Mohammed Faruq, MBBS, PhD
Genomics and Molecular Medicine, CSIR-Institute of Genomics and Integrative Biology (CSIR -IGIB), Mall Road,
Delhi 110007, India
E-mail: faruq.mohd@igib.res.in

Keywords: SCA12; autosomal dominant cerebellar ataxia; shortest pathogenic CAG repeats; cerebellum; *PPP2R2B*

Abbreviations: ICARS = International Cooperative Ataxia Rating Scale; IpA = intermediate pathogenic CAG alleles (43–50); PA = typical pathogenic length of CAG alleles (51); SCA12 = spinocerebellar ataxia type 12

Introduction

Spinocerebellar ataxia type 12 (SCA12) is a late onset autosomal dominant neurodegenerative disorder. Phenotypically, at disease onset, SCA12 manifests characteristic action tremors in the upper limbs, followed mainly by other movement abnormalities i.e. head tremor, dysarthria, and later during the course of disease progression, patients often develop gait ataxia (Holmes *et al.*, 2001; Srivastava *et al.*, 2001). Among other neurological deficits, pyramidal features, extrapyramidal abnormalities, chorea, dementia and cognitive declines have also been reported (Srivastava *et al.*, 2001). The disease exhibits inter/intra familial phenotypic heterogeneity (Holmes *et al.*, 2001). Brain imaging usually reveals both cerebral and cerebellar atrophy with relative sparing of brainstem, thalamus, basal ganglia and other subcortical brain regions (Holmes *et al.*, 2003). The age at disease onset is highly variable and ranges from 8–62 years, with the mean age of onset being 38 years (Holmes *et al.*, 2001). The causal mutation for SCA12 is the expansion of CAG repeats (>51 repeat units) in the 5'UTR of *PPP2R2B* gene (Holmes *et al.*, 1999). It is the second most common dominant ataxia in North India and almost uniquely observed in the Indian population. However, there are reports of SCA12 occurrence outside the Indian subcontinent as well: USA (the original family of American kindred with German descent in whom SCA12 was first described), Italy and the Chinese (Han) population (Holmes *et al.*, 1999; Jiang *et al.*, 2005; Brussino *et al.*, 2010; Li *et al.*, 2011). To date, the reported and clear pathological range for CAG repeats has been found to be 51–78 (Holmes *et al.*, 2001; Srivastava *et al.*, 2001; Bahl *et al.*, 2005), although there has been a recent report of identification of CAG-46 as the shortest pathogenic allele in *PPP2R2B* (Dong *et al.*, 2015). The unambiguous normal range of *PPP2R2B*-CAG has been found to be 4–31 repeats (Fujigasaki *et al.*, 2001; Srivastava *et al.*, 2001; Sulek *et al.*, 2004; Sulek-Piatkowska *et al.*, 2010; O'Hearn *et al.*, 2012; Merrill, 2012). From the earlier reports, concerns have remained regarding the cut-off pathogenic length for CAG repeats that are associated with SCA12 phenotype, namely (i) observation of two patients with late onset ataxia carrying 40 and 41 CAG repeats from the German population (Hellenbroich *et al.*, 2004); (ii) observation of 36 and 43 repeats in ataxic patients from the Czech population (Musova *et al.*, 2013); (iii) observation of one asymptomatic individual with 45 CAG repeats in the Indian population (Fujigasaki *et al.*, 2001); (iv) observation of 49 CAG alleles in a patient with phenotype of Creutzfeldt-Jacob Disease (CJD) (Hellenbroich *et al.*, 2004); and (v) the observation of CAG repeats 51 and 52 in Iranian patients with bipolar disorder (O'Hearn *et al.*, 2012). In this study, we report the clinical profiles of SCA12 patients with low abnormal CAG repeat length (CAG < 51) and compare their features with the patient group with defined minimum pathogenic length of CAG-51. This study provides the definition of minimum

pathogenic CAG allele causal for SCA12 phenotype and indicates the plausible pathogenic role of earlier reported low/intermediate CAG repeats in the range of 43–49 among ataxic patients from various global populations.

Materials and methods

The patients carrying *PPP2R2B*-CAG ≤ 51 ($n = 27$ from 25 families) were identified from the SCA12 patient group from our large scale effort for phenotype-genotype correlation in 125 unrelated SCA12 families. General demographics of these unrelated 124 index cases were as follows with mean (standard deviation, SD) and range for *PPP2R2B*-CAG expansion 56.5 (5.7), 43–73; age at onset [47 (10.3), 18–71 years]; and age at examination [53.2 (10.3), 23–74 years]. The selected individuals in the study population comprised 18 patients from 16 unrelated families (Supplementary material) who were identified to harbour intermediate *PPP2R2B*-CAG length [CAG (43–50)] and nine unrelated patients who were carriers of typical pathogenic threshold repeat length CAG (51) for SCA12. All the patients had manifestations of SCA12-like phenotype prior to genetic investigations (familial late onset progressive action tremor in hands and/or tremulous speech and/or head tremor and/or gait ataxia at the onset of disease and variable association of other neurological manifestations). Except for one patient, all others had a background of ethnicity as described earlier for SCA12 [an endogamous population from Haryana state of Northern India, IE-N-LP18 as described in the Indian Genome Variation Consortium (IGV) consortium study (2008)].

Clinical analysis included standard neurological examination of all probands and affected relatives by a team of neurologists. A detailed and comparative radiological investigation of brain was performed using images from 1.5 T MRI for patients harbouring different CAG alleles. Assessment of atrophic/degenerative pattern was evaluated using Koedam scores for parietal atrophy (Koedam *et al.*, 2011), medial temporal lobe atrophy (MTA) scale (Heo *et al.*, 2013), Fazekas scale for white matter lesions (Leaper *et al.*, 2001), global cortical atrophy (GCA) scale and cerebellar atrophy by visual assessment. Molecular analysis for the *PPP2R2B*-CAG repeat length estimation was done using fluorescence-based polymerase chain reaction (PCR) amplification with previously published primers (Srivastava *et al.*, 2001; Bahl *et al.*, 2005). The amplified fluorescent labelled PCR products were analysed by capillary electrophoresis on 3130xl ABI sequencer (Applied Biosystems). The sizing analysis for CAG length estimation was carried out by fragment analysis tool in GeneMapper® software v.4 (ABI). The confirmation of CAG repeat length was carried out by Sanger sequencing method by PCR using unlabelled primers (as previously described), followed by direct sequencing using ABI BigDye® chain terminator sequencing kit. We also later approached (by house visit) 11 other affected and unaffected siblings of the six kindreds (with CAG 43–50) for clinical and genetic assessment. All of the recruited patients had given their informed consent for participation in this study and the study was approved by the Institutional Ethics committees of the participating institutes.

Results

The general demographic details were as follows: the patient group with intermediate pathogenic CAG alleles (IpA, 43–50) with male:female ratio of 9:9, had [mean (SD), range] age at presentation [63.6 (6.8), 47–74 years]; age at onset [58.3 (8.2), 35–72 years] and disease duration [5.2 (3.2), 1–12 years], while the patients who were carriers for the typical pathogenic length (PA) of CAG-51 (male:female, 6:3) had [mean (SD), range] age at presentation [59.5 (11), 35–71 years], age at onset [54.11 (9.9), 34–66 years] and disease duration [5.4 (5.8), 1–20 years]. Among all the SCA12 patients, over and above the cerebellar features, various extracerebellar features including pyramidal features, extrapyramidal, urinary symptoms and peripheral neuropathy were also observed in a significant, but variable proportion (Table 1). We observed differences and overlaps in the clinical characteristics between these two groups (Table 1): (i) age at onset: the patient group with CAG < 51 had delayed mean (SD, range) age at onset 58.3 (8.2, 35–72) years than the patients with CAG-51, 54.11 (9.9, 34–66); (ii) neurological features: tremor and cerebellar ataxia were observed in near similar frequencies between the two groups; Babinski sign, nystagmus, dysarthria and urinary symptoms were observed with statistically non-significant higher frequency in the IpA group. However, in comparison with the earlier description by Srivastava *et al.* (2001) (patients with CAG range 56–69), the frequencies of various neurological signs were lower in both the IpA and PA groups. We observed a wide heterogeneity in the age at onset among patients harbouring the same repeat length, for CAG-45 (57–61 years), CAG-46 (51–67 years), CAG-47 (50–65 years), CAG-48 (35–53 years), CAG-49 (55–67 years) and CAG-50 (60–61 years). Similar to that of the PA group, we observed that in the IpA group, the most common symptom at onset was action tremor in the hand (55.5%) and if tremor were considered irrespective of anatomical location (including speech and head tremor) then it remains as a symptom at onset in 77% of the cases. Upper limb incoordination was observed as a symptom at onset in one individual and walking imbalance in the rest of the patients. However, frequencies observed were quite similar to those described earlier (67%) and those observed in patients with CAG-51 (67%). In 50% of the patients with CAG-51 or CAG < 51, tremor at its onset was asymmetric affecting either side unequally as per history. However, on examination, the severity observed was symmetric in most of the patients. All patients had hand tremor and/or gait ataxia on examination, except for one patient (Patient AT392/3905, Table 1), who, with CAG-16/47 and disease duration of 4 years, did not develop any other deficit except for head tremor. A general pattern of evolution of symptoms was tremor, followed by ataxia and speech slurring/tremor. Gait ataxia developed 1–5 years later after the onset of tremor (median 2 years). In addition, a weak negative correlation

(statistically non-significant) was observed between CAG length and the age at onset (Pearson correlation coefficient $r = -0.271$). However, an extended analysis in our larger cohort of 124 unrelated patients with SCA12 showed a statistically significant correlation between CAG repeats and age at onset with the following values, Pearson's r (-0.65), P -value $< 10^{-4}$.

Association of 43 CAG repeats with SCA12 phenotype

The proband of a three-generation pedigree (Fig. 1, Pedigree 872), was a 74-year-old female (Patient AT2058), who presented with asymmetric onset of tremor in the right hand, writing difficulty for the previous 2 years and developed gait ataxia a year later after tremor onset. Neurological examination revealed normal higher mental functions (normal Mini-Mental State Examination), finger–nose test showed gross dysmetria and tandem gait was impaired. Although the patient could still walk without support, her gait was clearly abnormal and irregular. Eye signs were normal except for broken pursuits. The patient had a moderate degree of bradykinesia. Deep tendon reflexes were normal except for reduced ankle jerk. Sensory examination revealed decreased vibration sense in lower limb (LL) > upper limb (UL). No extrapyramidal features, no fasciculations and no muscle atrophy were present. MRI brain scan showed both cerebral and cerebellar atrophy (Fig. 2A–C). Sensory and motor nerve conduction studies were normal. A total score of 15 was obtained on the ataxia severity rating scale. Regular follow-up (2011–15) showed progressively increasing disease and severity scores assessed by the International Cooperative Ataxia Rating Scale (ICARS). Her family history was positive for tremor/ataxia in multiple individuals (Fig. 1, Pedigree 872). Among other members of the family who were available for genetic and clinical analysis, two affected siblings (Patients AT894 and AT2059) were also study subjects (Table 1). We later analysed three unaffected individuals of this family by house visit, for clinical assessment and genetic analysis. Three of the asymptomatic individuals had no neurological manifestation and their genetic analysis revealed CAG repeats 14/39 for Patient AT4388 (age 89 years) and Patient AT4389 (age 82 years). The remaining sibling Patient AT4387 (age 77 years) was found to be a carrier of 17/39 CAG genotype (Fig. 1, Pedigree AT872).

Effect of biallelic CAG repeat expansion on SCA12 phenotype

We identified two individuals with biallelic expansion, one of whom (Patient AT476/1498) harboured 45/45 CAG alleles and the other carried a CAG-42/51 genotype (Patient AT648/2017) (Fig. 1, Pedigree AT648). The latter case (CAG-42/51) was a 55-year-old female who had developed

Table 1 Clinical features of patients with CAG > 51 and comparison with patients carrying CAG-51

| Parameters | Patient group CAG = 51 (43–50) | Patient group CAG < 51 (2001) | Srivastava et al. (2001) | Patient Identification (ID) (Family ID/Sample ID) | | | | | | | | | | | | | | | | A- T190- 5/ 3514 |
|------------------------------|--------------------------------------|-------------------------------------|--------------------------------|---|----------------|-----------------|----------------|----------------|----------------|----------------|----------------|---------------|---------------|-----------------|----------------|----------------|----------------|----------------|-----------------|---------------------------|
| | | | | AT872/ 2058 | AT630/ 1683 | AT1005/ 2251 | AT476/ 1498 | AT899/ 2113 | AT610/ 1653 | AT356/ 1214 | AT392/ 1305 | AT872/ 894 | AT273/ 908 | AT3500/ 4301 | AT632/ 1584 | AT940/ 2177 | AT328/ 1037 | AT872/ 2059 | AT1403/ 2800 | AT928/ 2165 |
| Male:Female ratio | 6:3 | 9:9 | 5:1 | F | M | M | F | F | F | M | F | M | M | F | M | M | M | F | F | M |
| Age at examination, in years | 59.5 (11), 35–71 | 63.5 (6.8), 47–74 | | 74 | 60 | 66 | 63 | 55 | 72 | 61 | 68 | 72 | 57 | 68 | 60 | 47 | 60 | 70 | 63 | 67 |
| mean (SD), range | | | | | | | | | | | | | | | | | | | | |
| Age at onset, in years | 54.11 | 58.3 (8.2), 35–72 | 37.1 | 72 | 57 | 60 | 61 | 51 | 67 | 60 | 64 | 65 | 50 | 56 | 53 | 35 | 56 | 67 | 55 | 61 |
| years mean | | | | | | | | | | | | | | | | | | | | |
| (SD), range | | | | | | | | | | | | | | | | | | | | |
| Disease duration | 5.4 (5.8) | 5.2 (3.2) | | 2 | 3 | 6 | 2 | 4 | 5 | 1 | 4 | 7 | 7 | 12 | 7 | 12 | 4 | 3 | 8 | 6 |
| mean (SD) | | | | | | | | | | | | | | | | | | | | |
| CAG length mean (SD) | 51 | 47(2), 43–50 | 62.6, 56–69 | 14/43 | 13/45 | 13/45 | 45/45 | 9/46 | 10/46 | 9/46 | 16/47 | 17/47 | 15/47 | 10/47 | 14/48 | 9/48 | 9/49 | 17/49 | 10/49 | 9/50 |
| First symptom, action tremor | 67 | 56 | 67 | HT | GA | HT | SpT | HT | SpT | UL-In | HdT | HT | HT | HT | HT | GA | HdT | HT | HT | HT |
| hand, % | | | | | | | | | | | | | | | | | | | | |
| Symptom evolution | | | | | | | | | | | | | | | | | | | | |
| Hand tremor | 100 | 88(16/18) | 67 | T > At > Sp | At > T | At > T | Sp > T | At > T | Sp > T | At > T | HdT | T > T | T | T > Sp | T | At > T | HdT > T | T | T > T | T > At |
| Upper limb ataxia | 100 | 83(15/18) | 100 | + | + | + | + | + | + | + | + | + | + | + | + | + | + | + | + | + |
| Gait ataxia | 88 | 88(16/18) | 100 | + | + | + | + | + | + | + | + | + | + | + | + | + | + | + | + | + |
| Dysarthria/speech | 44.44 | 72(13/18) | 100 | + | + | + | + | + | + | + | + | + | + | + | + | + | + | + | + | + |
| tremor | | | | | | | | | | | | | | | | | | | | |
| Tremor | 55.5 | 61(11/18) | 67 | + | + | + | + | + | + | + | + | + | + | + | + | + | + | + | + | + |
| (head/jaw/face) | | | | | | | | | | | | | | | | | | | | |
| Hyperreflexia | 66.66 | 50(8/16) | 83 | – | – | na | + | + | + | na | – | – | – | + | + | + | – | + | – | – |
| Babinski sign | 13 | 50(8/16) | 33 | + | + | na | + | + | – | na | – | – | – | + | – | – | – | + | + | + |
| Extrapyramidal | 55.55 | 47(8/17) | 33 | + | + | na | + | + | – | – | – | + | – | – | – | – | – | + | + | + |
| Peripheral neuropathy | 20(1/5) | 18(2/11) | 83 | – | – | na | – | na | na | na | na | – | + | – | na | – | + | – | – | na |
| Nystagmus | 28.57 | 35(6/17) | 17 | – | + | na | + | – | + | – | – | – | – | + | + | + | – | – | – | – |
| Broken pursuit | 14.28 | 41(7/17) | 33 | – | – | na | + | – | – | – | – | + | – | + | – | – | + | + | + | + |
| Slow saccades | 14.28 | 23(4/17) | 17 | – | – | na | + | – | – | – | – | + | – | – | – | – | + | – | – | – |
| Urinary symptoms | 40(2/5) | 45(5/11) | nr | – | + | na | na | – | – | na | na | na | na | – | + | + | na | + | – | – |
| CT/MRI | 80(4/5) | 56(10/18) | 83 | CCbA, WM | CCbA, WM | na | CCbA | na | na | CbA | CA | CA | CA | CA | na | CCbA, WM | na | na | CCbA | na |
| (CCbA/CA) | | | | | | | | | | | | | | | | | | | | |
| ICARS | | | | 15 | 35 | na | 27 | 18 | na | na | na | na | na | 21 | 40 | 26 | na | 16 | na | 33 |

At = ataxia; CCbA = cerebello-cerebellar atrophy; CA = cerebral atrophy; F = Female; HdT = head tremor; T = tremor; HT = hand tremor; GA = gait ataxia; M = Male; na = not available; Sp = speech impairment; WMH = white matter hyperintensities; + = presence of that feature; – = absence of that feature. Text in bold indicates CAG repeat lengths for the respective patient.

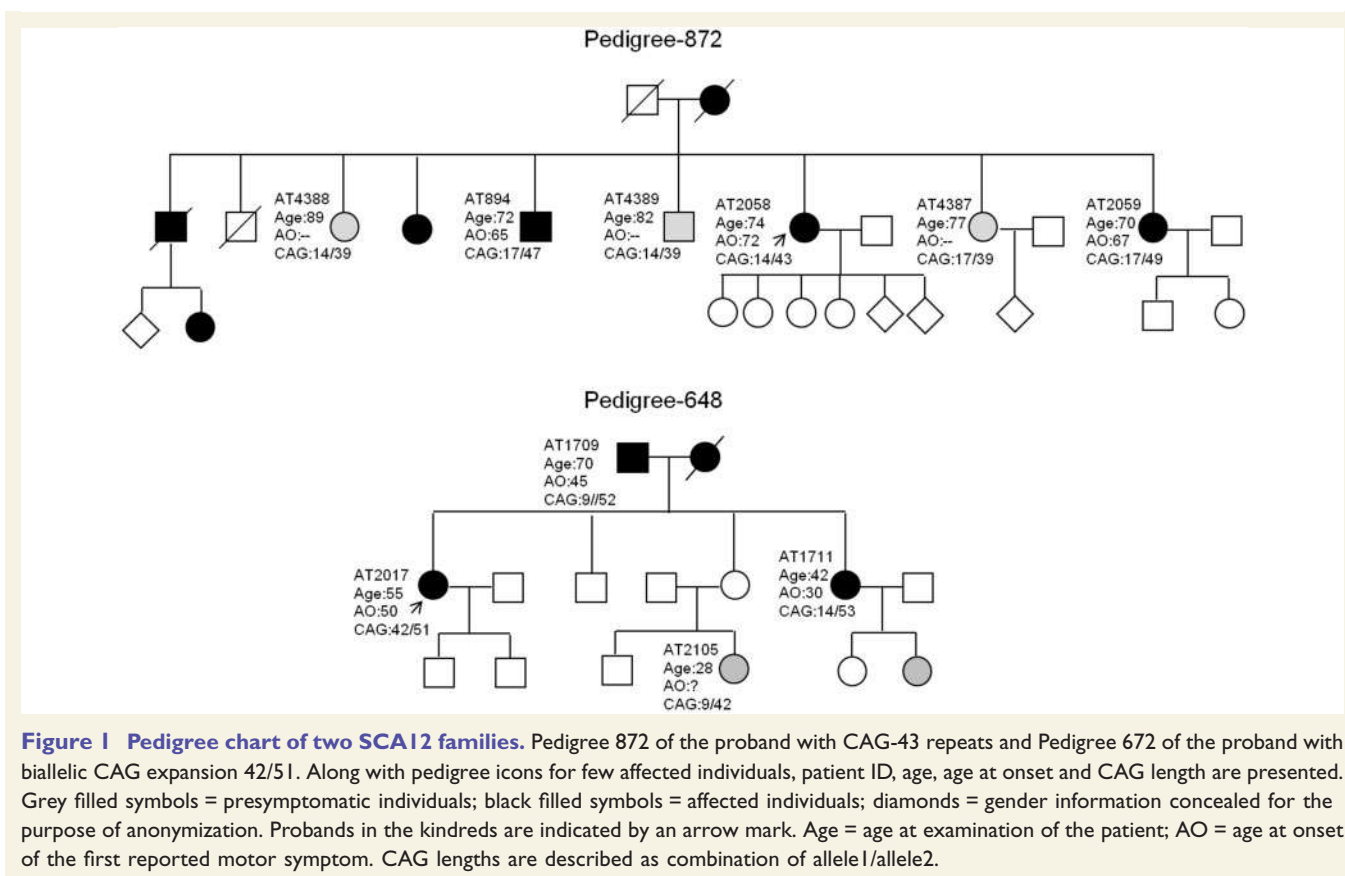


Figure 1 Pedigree chart of two SCA12 families. Pedigree 872 of the proband with CAG-43 repeats and Pedigree 672 of the proband with biallelic CAG expansion 42/51. Along with pedigree icons for few affected individuals, patient ID, age, age at onset and CAG length are presented. Grey filled symbols = presymptomatic individuals; black filled symbols = affected individuals; diamonds = gender information concealed for the purpose of anonymization. Probands in the kindreds are indicated by an arrow mark. Age = age at examination of the patient; AO = age at onset of the first reported motor symptom. CAG lengths are described as combination of allele1/allele2.

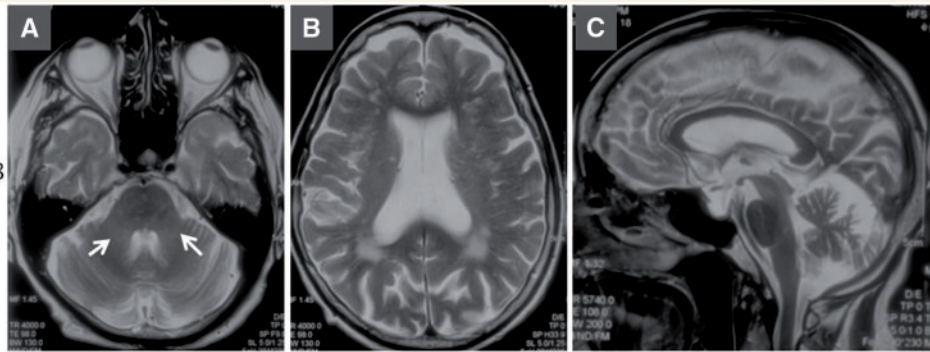
progressive asymmetric hand tremors (right > left) over the past 5 years and gait ataxia for 3 years. Nystagmus, broken pursuits, hyperreflexia and Babinski sign were observed and she had a moderate degree of intention tremor and gait ataxia on examination. Radiologically, no obvious atrophic changes were observed in the MRI brain scan. The proband had a strong family history (Fig. 1, Pedigree B) with both her parents being symptomatic for tremor/ataxia of SCA12 phenotype. Her father (Patient AT1709, 9/51 CAG repeats) harboured and had disease onset at 45 years of age, and one of her younger symptomatic siblings (Patient AT1711, 14/53 CAG) had disease onset at 30 years. An asymptomatic niece (Patient AT2105) carried 9/42 CAG repeats (for asymptomatic screening) and at the age of 28 years, showed minimal hand tremor, which was elicited objectively but no subjective complaints were made. Overall, when the homozygous case (Patient AT2017) was compared with individuals carrying heterozygous 51 repeats, no clinical differences were observed for either age at onset [patient, 50 years, PA (CAG-51 group) mean 54.6, range 34–66] or disease severity [in this patient ICARS scores were 7 with disease duration of 5 years, while a heterozygous individual, Patient AT1358 (10/51), had ICARS score of 18 with disease duration of 1 year, data not shown]. When compared with the individuals harbouring heterozygous 51 CAG, a mild course and later onset were observed. Similarly, we compared another

individual with CAG genotype of 45/45 (Patient AT476/1498) with heterozygous subjects with CAG-13/45 each (Patients AT630/1683 and AT1005/2251, Table 1). Patient AT476/1498 had disease onset at 61 years with tremulous speech as the onset symptom, while the heterozygous individuals with CAG-45 had age of onset at 57 and 60 years, respectively. The disease severity analysed using ICARS for Patient AT630/1683 was 35 with 3 years of disease duration, whereas, the 45/45 homozygous subject had a comparable severity score of 27 with 2 years of disease duration.

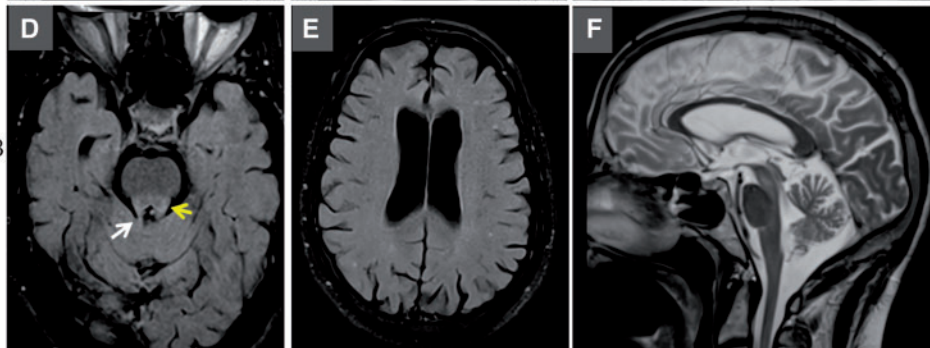
Radiological findings

In general, the brain MRI findings of patients showed patterns of variable degree of cortical atrophy and cerebellar atrophy in both groups of patients (IpA or PA); however, cortical atrophy was more pronounced than cerebellar atrophy. We also comparatively analysed the MRI images of patients carrying different CAG length 43–51 using visual assessment and standard scoring tools (Fig. 2 and Table 2). We observed that on every applied scale for assessment of atrophic changes, except for two patients, all showed some varying degree (mild-to-moderate) of cortical atrophy greater than cerebellar atrophy (Table 2). The two patients, who interestingly harbour typical pathogenic lengths CAG-51 (Patient AT1358) and biallelic expansion 42/51 (Patient AT648/2017) and disease duration of 2 and 5

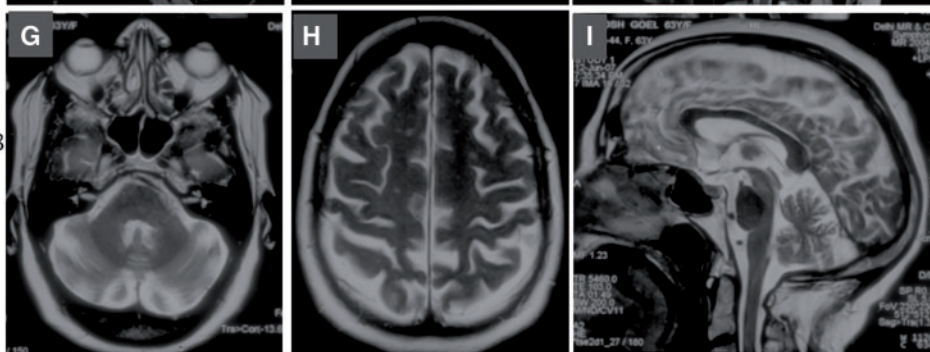
PID: AT872/2058
Age: 74 yrs
AO: 72 yrs
CAG-14/43



PID: AT630/1683
Age: 60 yrs
AO: 57 yrs
CAG-13/45



PID: AT476/1498
Age: 63 yrs
AO: 61 yrs
CAG-45/45



PID: AT3500/4301
Age: 68 yrs
AO: 56 yrs
CAG-10/47

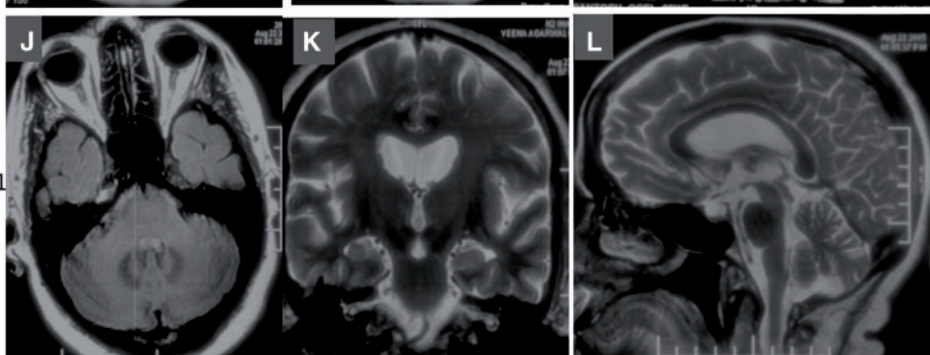
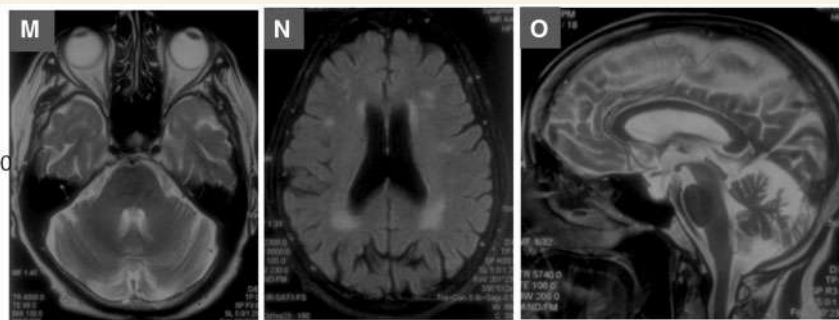
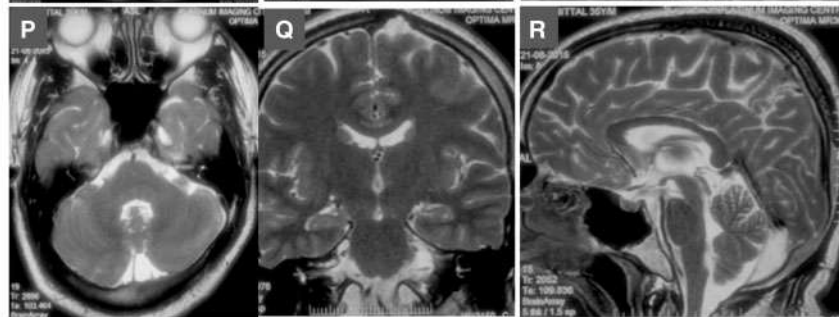


Figure 2 Representative brain MRI images of selected patients with different CAG length. MRI brain (A–C) of Patient AT872/2058 carrying CAG-14/43. Axial T₂-weighted images (A and B) showing cortical atrophy and white matter hyperintensities in bilateral middle cerebellar peduncle (arrows). (C) Sagittal T₂-weighted image showing prominent cerebellar atrophy. (D–F) MRI of Patient AT630/1683 carrying CAG-13/45. (D) Axial T₁-weighted image showing white matter hyperintensities in dorsal tegmentum (yellow arrow) and in superior cerebellar peduncle (white arrow) and mild degree of temporal lobe atrophy. (E) Fluid attenuation inversion recovery (FLAIR) axial image showing mild degree of parietal lobe atrophy. (F) Sagittal T₂-weighted image showing mild degree of cerebellar atrophy. (G–I) MRI of Patient AT476/1498 carrying homozygous CAG-45 repeats. (G and H) Axial T₂-weighted images showing moderate degree of parietal lobe atrophy, multiple punctuate lesion and (I) sagittal T₂-weighted image showing mild degree of cerebellar atrophy. (J–L) Brain MRI of Patient AT3500/4301 carrying CAG-10/47. Axial T₂-weighted (J), coronal T₂-weighted (K) and sagittal T₂-weighted (L) images showing mild generalized cortical atrophy and no cerebellar atrophy. (M–O) MRI brain of Patient AT1403/2800 carrying CAG-10/49. Axial T₂-weighted (M) and axial FLAIR (N) images showing moderate degree of cortical atrophy and diffuse multiple punctuate lesions and sagittal T₂-weighted (O) image showing mild degree of cerebellar atrophy. (P–R) MRI brain of patient carrier of heterozygous typical pathogenic length CAG-51. Axial T₂-weighted (P), coronal T₂-weighted (Q) and sagittal T₂-weighted (R) images showing normal-appearing brain parenchyma. (S–U) MRI brain of patient carrier of biallelic repeat expansion (Patient AT648/2017) CAG-42/51. Axial T₂-weighted (S), coronal T₂-weighted (T) and sagittal T₂-weighted (U) images showing normal-appearing brain parenchyma.

PID: AT1403/2800
Age: 63 yrs
AO: 55 yrs
CAG-10/49



PID: AT1358
Age: 31 yrs
AO: 29 yrs
CAG-10/51



PID: AT648/2017
Age: 55 yrs
AO: 50 yrs
CAG-42/51

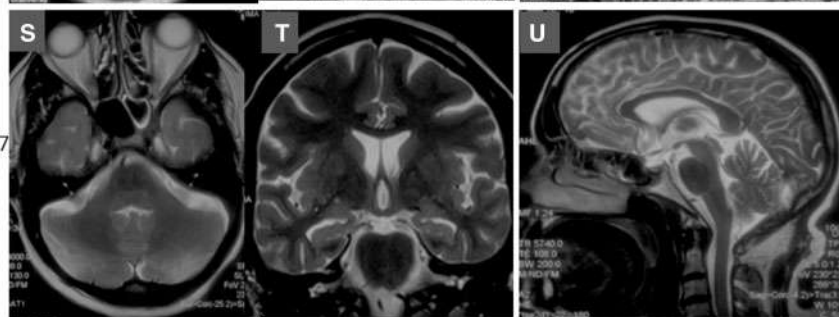


Figure 2 Continued.

years, respectively, did not show any atrophic changes in either the cortical or cerebellar region. For other patients from the IpA group, we found that there was no correlation with disease severity or disease duration and atrophic changes in the brain. Unexpectedly, a 74-year-old patient (Patient AT872/AT2058) with the lowest abnormal CAG-43 expansion, showed a moderate degree of cortico-cerebellar atrophy, probably reflecting contribution of age-related changes in the brain in final radiological interpretation. We also observed white matter lesions in four patients (Patients AT476/1498, AT872/AT2058, AT1403/2800 and AT3500/4301) on the Fazekas scale, with prominent T₂ white matter hyperintensities (WMHs) in bilateral middle and superior cerebellar peduncle (Patient AT872/AT2058; CAG-14/43 and Patient AT630/1683; CAG-13/45) and additional WMHs in dorsal tegmentum in Patient AT630/1683.

Discussion

Certain spinocerebellar ataxia subtypes caused by triplet/tandem repeat expansion exhibit a differential prevalence with respect to ethnic and geographical background,

mainly due to founder mutations for specific SCA loci (Duenas *et al.*, 2006). Globally, apart from some common SCA subtypes (SCA1–3), few ataxia subtypes have a population-specific over-representation e.g. SCA10 in Brazil and Mexico, DRPLA in Japan and SCA12 in India (Duenas *et al.*, 2006; Faruq *et al.*, 2009). In India, SCA12 is mostly confined to one endogamous population; however, ~5–8% of families with SCA12 have been found from other ethnic communities (unpublished observation from our SCA patient cohort). Clinically, the SCA12 phenotype has a unique manifestation of prominent action tremor of hands, which distinguishes it from other SCA subtypes. It does, however, resemble the phenotype of Fragile X-associated tremor/ataxia syndrome (FXTAS) (Faruq *et al.*, 2014). Atypical neurological presentations including bipolar psychiatric disease and amyotrophic lateral sclerosis have been associated with PPP2R2B-CAG expansion (both pathogenic and intermediate length CAG repeats) (Hellenbroich *et al.*, 2004; O'Hearn *et al.*, 2012; Musova *et al.*, 2013). In this study, we aimed to identify the clinical and genetic behaviour of patients who were initially ascribed a clinical diagnosis for SCA12 and were

Table 2 MRI-based radiological evaluation of brain and clinical correlation

| Patient ID | Age | AO | Duration | ICARS | CAG | Koedam score | MTA | Fazekas scale | GCA | Cerebellar atrophy | White matter changes |
|--------------------------|-----|----|----------|-------|-------|--------------|-----|---------------|-----|--------------------|--|
| AT872/2058 | 74 | 72 | 2 | 15 | 43 | 2 | 0 | 2 | 2 | ++ | T ₂ hyperintensity in b/l middle and superior cerebellar peduncle |
| AT630/1683 | 60 | 57 | 3 | 35 | 45 | 1 | 2 | 0 | 1 | + | T ₂ hyperintensity in b/l superior cerebellar peduncles, dorsal tegmentum |
| AT476/1498 | 63 | 61 | 2 | 27 | 45/45 | 2 | 0 | 1 | 1 | + | — |
| AT3500/4301 | 68 | 56 | 12 | 21 | 47 | 0 | 0 | 1 | 1 | — | — |
| AT1403/2800 | 63 | 55 | 8 | | 49 | 2 | 2 | 1 | 2 | + | — |
| AT1905/3514 ^a | 62 | 60 | 2 | 15 | 50 | | | | 1 | — | — |
| AT1358 | 31 | 29 | 2 | 18 | 51 | 0 | 0 | 0 | 0 | — | — |
| AT648/2017 | 55 | 50 | 5 | 7 | 42/51 | 0 | 0 | 0 | 0 | — | — |

^aBased on plain CT scan of head.

Age = age at examination in years; AO = age at onset of movement disorder; Koedam score for parietal lobes atrophy: Grade 0, no cortical atrophy; Grade 1, mild parietal atrophy; Grade 2, substantial parietal atrophy; Grade 3, end-stage 'knife-blade' atrophy; MTA (medial temporal lobe atrophy): score 0, no atrophy; score 1, only widening of choroid fissure; score 2, a widening of temporal horn of lateral ventricle; score 3, moderate loss of hippocampal volume (decrease in height); score 4, severe volume loss of hippocampus; Fazekas Scale: Fazekas 0, none or a single punctate WMH lesion; Fazekas 1, multiple punctate lesions; Fazekas 2, beginning confluency of lesions (bridging); Fazekas 3, large confluent lesions; GCA-scale (Global Cortical Atrophy): 0, no cortical atrophy; 1, mild atrophy opening of sulci; 2, moderate atrophy, volume loss of gyri; 3, severe (end-stage) atrophy, 'knife blade' atrophy. b/l = bilateral; — = absent; + = mild; ++ = moderate.

later identified as carrying varying lengths of CAG repeats in the *PPP2R2B* gene in the range of 43–50 ($n = 18$), which we refer to as intermediate length pathogenic repeats (IpA). We then compared their features with patients who harboured minimum definitive pathogenic length alleles (PA, CAG-51, $n = 9$) in order to understand the relevance of intermediate CAG length with respect to typical SCA12 phenotype. We observed that in the IpA group of patients, the mean age at onset was 58 years (with a wide range, 35–72 years) with no clear correlation with CAG length, which is contrary to the observed negative correlation of CAG and age and onset in the larger dataset of SCA12 patients ($n = 124$). Hence, other factors may have a significant contribution towards the age at onset in the IpA patient group. However, irrespective of age at disease onset, the phenotypes show typical features of SCA12. The clinical and genetic features in one kindred (Patient AT872) were of particular interest, where the proband and her two siblings with typical SCA12 phenotype carried varying CAG lengths, 43, 47 and 49. None of the three unaffected siblings (neurologically normal at older age than proband's age) carried these repeat lengths and interestingly were all heterozygous carriers of 39 repeats. Thus, with the proband with CAG-43 repeats (Patient AT872/2058, age at onset 72 years) with observed clinical features suggestive of typical SCA12 phenotype as also indicated by radiological manifestations and the absence of any SCA12 features in CAG-39 repeat carriers, it is likely that 43-CAG is the minimum pathogenic length for the SCA12 phenotype in this family. In addition, we would like to mention that the previously reported ataxia patients with CAG repeats in the range of 36 and 43 repeats from the Czech population were younger in age than our proband (Musova *et al.*, 2013). They may

not have manifested the typical SCA12 phenotype at that age or presented with atypical features of SCA12. Other than this, from a molecular biology point of view, it has also previously been shown that expanded CAG repeats (with sequence context), when placed in the promoter region of a luciferase reporter, enhance luciferase activity in a length-dependent manner (Lin *et al.*, 2010; O'Hearn *et al.*, 2015). That study also showed that CAG length of 35 as minimum can increase luciferase reporter activity at a transcriptional level. Thus, taking all this evidence into account, we consider that CAG-43 repeats can lead to molecular pathological events resulting in neurodegeneration and can be considered as the shortest pathogenic length for the SCA12 phenotype. We also agree that more evidence will be necessary to observe the phenotypic variability associated with CAG-43 or incomplete penetrance.

Other than CAG-43, we tried to analyse other CAG IpA (45–50) in the available family members of the respective kindreds ($n = 6$). In a kindred with heterozygous CAG-45 (Patient AT1005) (Supplementary material), the asymptomatic sibling (age 63 years) had CAG-42. Another kindred (AT3500) with index patient (heterozygous CAG-47) had two other affected siblings (twins) who were found to have CAG-46 and CAG-47 with age of disease onset at 63 and 62 years, respectively. For four other kindreds, CAG repeat size data were available for offspring (who were recruited as a part of presymptomatic testing). However, having their asymptomatic status and younger age, these individuals will not be suitable for studying the incomplete penetrance (Supplementary material). We can therefore state that, the previously described Indian subject with heterozygous CAG-45 may develop disease at a later point, as we noted large heterogeneity in the age at onset of our

SCA12 patients with CAG-45 and other intermediate alleles. The cases described in the German population who were found to carry 40 and 41 CAG repeats (Hellenbroich *et al.*, 2004) and were also shown to manifest late onset ataxias, may also have pathogenic significance in the context of SCA12 as shown that luciferase activity is enhanced by a minimum of 35 CAG repeats. In the present study cohort, we also observed a presymptomatic individual, a 28-year-old female (Patient AT2105), who carried CAG 9/42 (Fig. 1, Pedigree 648) and had manifested tremor upon objective assessment, which will require follow-up to confirm its pathogenicity.

We also observed that SCA12 biallelic CAG expansion exerts no added clinical severity or phenotypic modulation. It has also been observed in other triplet repeat expansion disease cases that homozygosity may or may not influence overall severity, which is contrary to the hypothesis of toxic accumulation of RNA or protein species in the form of inclusion and its role as a key governing mechanism of neurodegeneration in triplet repeat disorders (Duenas *et al.*, 2006).

The radiological findings are suggestive of clinical or sub-clinical manifestations of diffuse degenerative programme in the brain of patients harbouring CAG 43–50, showing no clear correlation with phenotypic manifestations. The findings corroborate with neuropathological changes as reported by a post-mortem study of brain tissue, where mild cerebellar atrophy was observed as compared to the cerebral cortical atrophy (O’Hearn *et al.*, 2015). We also observed white matter changes in neural connections (superior and middle cerebellar peduncles) of cerebellum in two MRIs. Two reports documented MRI white matter abnormalities (white matter changes in the cerebral cortex) and another showed reduced fractional anisotropy in cerebral cortex and cerebellar vermis in patients and presymptomatic subjects (Li *et al.*, 2014; Hu *et al.*, 2015). Radiologically, no gross relation was observed with clinical manifestations in our patients, but based on reported literature and our findings, it can be speculated that tremor and ataxia symptoms are initial and ‘tip of the iceberg’ features of major pathological changes, which would evolve with disease course. Grossly, cerebellum appears to be less involved at least in its cortical areas as also observed in a pathological study; however, more evidence is needed to understand the microstructural changes in the brain of SCA12 patients, reflected as clinical findings. It can also be speculated that cerebellar degeneration may be representative of secondary changes as to primary degeneration affecting cerebral cortex and its connection to cerebellum. To date, no evidence is available to document the tremorigenic centre in SCA12; however, the characteristic hand tremor action and the association of head tremor, voice tremulousness and late development of gait ataxia along with radiological findings (white matter changes in the cerebellum and diffuse brain atrophy), bring it more closely towards FXTAS or essential tremor phenotypically. The presence of extrapyramidal and

pyramidal features, however, allow for distinction from essential tremor and FXTAS.

Conclusively, we present the observed typical clinical behaviour of intermediate length of *PPP2R2BB*-CAG towards SCA12 phenotype with large variability in the age at onset. Overall, 43 CAG repeats can be considered as the shortest CAG length towards SCA12 pathogenicity and also as the diagnostic threshold. The diagnostic threshold can still be lower (CAG-40) or even lower size alleles (CAG 36–40) may be pathogenic with reduced or age-dependent disease penetrance. We also emphasize that SCA12 mutation may not be restricted only to a few populations, rather at this locus (SCA12) recurrence of mutation will be the case in different geographic regions and due to stable nature of CAG repeats larger pathogenic mutation length are not observed widely. Among other geographical areas, there may be population level representation of large normal or intermediate alleles of *PPP2R2B*-CAG and so will be the presence of SCA12 as indicated in previous reports.

Acknowledgements

We are highly obliged to all the participating family members for cooperation and patience in clinical and genetic investigations till the end of the study. We sincerely thank Sunil Shakya, Varun Suroliya, Istaq Ahmad and Akhilesh Kumar Sonakar for providing their assistance in DNA extraction from saliva samples followed by CAG repeat length estimation by PCR and fragment analysis on ABI3130xl capillary electrophoresis instrument. We thank again Akhilesh kumar Sonakar for his technical assistance in patient recall, follow-up and obtaining investigational records from the patient and family members. We express our sincere thanks to Mr Aniket Bhattacharya, Senior research fellow (CSIR) for providing critical review of the manuscript and proof-reading of the article.

Funding

The financial support for the study was obtained from Council of Scientific and Industrial Research (CSIR) funded projects: GenCODE (BSC0123) and Extramural grant for AKS from CSIR funded project/scheme no. 60(0103)/13/EMR-II.

Supplementary material

Supplementary material is available at *Brain* online.



References

- Bahl S, Virdi K, Mittal U, Sachdeva MP, Kalla AK, Holmes SE, et al. Evidence of a common founder for SCA12 in the Indian population. *Ann Hum Genet* 2005; 69: 528–34.

- Brussino A, Graziano C, Giobbe D, Ferrone M, Dragone E, Arduino C, et al. Spinocerebellar ataxia type 12 identified in two Italian families may mimic sporadic ataxia. *Mov Disord* 2010; 25: 1269–73.
- Dong Y, Wu JJ, Wu ZY. Identification of 46 CAG repeats within PPP2R2B as probably the shortest pathogenic allele for SCA12. *Parkinsonism Relat Disord* 2015; 21: 398–401.
- Duenas AM, Goold R, Giunti P. Molecular pathogenesis of spinocerebellar ataxias. *Brain* 2006; 129: 1357–70.
- Faruq M, Scaria V, Singh I, Tyagi S, Srivastava AK, Mukerji M. SCA-LSVD: a repeat-oriented locus-specific variation database for genotype to phenotype correlations in spinocerebellar ataxias. *Hum Mutat* 2009; 30: 1037–42.
- Faruq M, Srivastava AK, Suroliya V, Kumar D, Garg A, Shukla G, et al. Identification of FXTAS presenting with SCA 12 like phenotype in India. *Parkinsonism Relat Disord* 2014; 20: 1089–93.
- Fujigasaki H, Verma IC, Camuzat A, Margolis RL, Zander C, Lebre AS, et al. SCA12 is a rare locus for autosomal dominant cerebellar ataxia: a study of an Indian family. *Ann Neurol* 2001; 49: 117–21.
- Hellenbroich Y, Schulz-Schaeffer W, Nitschke MF, Köhnke J, Händler G, Bürk K, et al. Coincidence of a large SCA12 repeat allele with a case of Creutzfeld-Jacob disease. *J Neurol Neurosurg Psychiatry* 2004; 75: 937–8.
- Heo JH, Kim MK, Lee JH, Lee JH. Usefulness of medial temporal lobe atrophy visual rating scale in detecting alzheimer's disease: preliminary study. *Ann Indian Acad Neurol* 2013; 16: 384–7.
- Holmes SE, Hearn EO, Ross CA, Margolis RL. SCA12: an unusual mutation leads to an unusual spinocerebellar ataxia. *Brain Res Bull* 2001; 56: 397–403.
- Holmes SE, O'Hearn E, Margolis RL. Why is SCA12 different from other SCAs? *Cytogenet Genome Res* 2003; 100: 189–97.
- Holmes SE, O'Hearn EE, McInnis MG, Gorelick-Feldman DA, Kleiderlein JJ, Callahan C, et al. Expansion of a novel CAG trinucleotide repeat in the 5' region of PPP2R2B is associated with SCA12. *Nat Genet* 1999; 23: 391–2.
- Hu T, Zhao B, Wei QQ, Shang H. Unusual cerebral white matter change in a Chinese family with Spinocerebellar ataxia type 12. *J Neurol Sci* 2015; 349: 243–5.
- IGV consortium. Genetic landscape of the people of India: a canvas for disease gene exploration. *J Genet* 2008; 87: 3–20.
- Jiang H, Tang B, Xu B, Zhao GH, Shen L, Tang JG, et al. Frequency analysis of autosomal dominant spinocerebellar ataxias in Han population in the Chinese mainland and clinical and molecular characterization of spinocerebellar ataxia type 6 [in Chinese]. *Zhonghua Yi Xue Yi Chuan Xue Za Zhi* 2005; 22: 1–4.
- Koedam EL, Lehmann M, van der Flier WM, Scheltens P, Pijnenburg YA, Fox N, et al. Visual assessment of posterior atrophy development of a MRI rating scale. *Eur Radiol* 2011; 21: 2618–25.
- Leaper SA, Murray AD, Lemmon HA, Staff RT, Deary IJ, Crawford JR, et al. Neuropsychologic correlates of brain white matter lesions depicted on MR images: 1921 Aberdeen Birth Cohort. *Radiology* 2001; 221: 51–5.
- Li H, Ma J, Zhang X. Diffusion tensor imaging of spinocerebellar ataxia type 12. *Med Sci Monit* 2014; 20: 1783–91. doi: 10.12659/MSM.891104.
- Li H, Lei J, Ma J, Yu J, Zhang X. Gene mutation and clinical characteristics of a Chinese Uyghur family with spinocerebellar ataxia type 12 [in Chinese]. *Zhonghua Yi Xue Yi Chuan Xue Za Zhi* 2011; 28: 137–41.
- Lin CH, Chen CM, Hou YT, et al. The CAG repeat in SCA12 functions as a cis element to up-regulate PPP2R2B expression. *Hum Genet* 2010; 128: 205–12.
- Musova Z, Sedlacek Z, Mazanec R, Klempir J, Roth J, Plevova P, et al. Spinocerebellar ataxias type 8, 12, and 17 and dentatorubro-pallidolysian atrophy in Czech ataxic patients. *Cerebellum* 2013; 12: 155–61.
- O'Hearn E, Holmes SE, Margolis RL. Spinocerebellar ataxia type 12. *Handb Clin Neurol* 2012; 103: 535–47. doi: 10.1016/B978-0-444-51892-7.00034-6.
- O'Hearn EE, Hwang HS, Holmes SE, Rudnicki DD, Chung DW, Seixas AI, et al. Neuropathology and cellular pathogenesis of spinocerebellar ataxia type 12. *Mov Disord* 2015; 30: 1813–24.
- Merrill RA, Slupe AM, Strack S. Spinocerebellar ataxia type 12 (SCA 12): clinical features and pathogenetic mechanisms. 2012, Spinocerebellar Ataxia Dr. José Gazulla (Ed.), InTech, DOI: 10.5772/29072.
- Srivastava AK, Choudhry S, Gopinath MS, Roy S, Tripathi M, Brahmachari SK, et al. Molecular and clinical correlation in five Indian families with spinocerebellar ataxia 12. *Ann Neurol* 2001; 50: 796–800.
- Sulek A, Hoffman-Zacharska D, Bednarska-Makaruk M, Szirkowiec W, Zaremba J. Polymorphism of trinucleotide repeats in non-translated regions of SCA8 and SCA12 genes: allele distribution in a Polish control group. *J Appl Genet* 2004; 45: 101–5.
- Sulek-Piatkowska A, Zdzenicka E, Raczynska-Rakowicz M, Krysa W, Rajkiewicz M, Szirkowiec W, et al. The occurrence of spinocerebellar ataxias caused by dynamic mutations in Polish patients. *Neurol Neurochir Pol* 2010; 44: 238–45.

ORIGINAL RESEARCH

Biallelic cGMP-dependent type II protein kinase gene (*PRKG2*) variants cause a novel acromesomelic dysplasia

Francisca Díaz-González,^{1,2} Saruchi Wadhwa,³ Maria Rodriguez-Zabala,^{1,4} Somesh Kumar,⁵ Miriam Aza-Carmona,^{1,2,4} Lucia Sentchordi-Montané,^{1,2,6,7} Milagros Alonso,⁸ Istaq Ahmad,³ Sana Zahra,³ Deepak Kumar,³ Neetu Kushwah,³ Uzma Shamim,³ Haseena Sait,⁵ Seema Kapoor,⁵ Belen Roldán,⁸ Gen Nishimura,⁹ Amaka C Offiah ^{10,11} Mohammed Faruq,³ Karen E. Heath ^{1,2,4}

► Additional material is published online only. To view, please visit the journal online (<http://dx.doi.org/10.1136/jmedgenet-2020-107177>).

For numbered affiliations see end of article.

Correspondence to

Dr Karen E. Heath, INGEMM, Hospital Universitario La Paz, Madrid 28046, Spain; karen.heath@salud.madrid.org

MF and KEH are joint senior authors.

Received 18 May 2020
Revised 22 September 2020
Accepted 23 September 2020



© Author(s) (or their employer(s)) 2020. No commercial re-use. See rights and permissions. Published by BMJ.

To cite: Díaz-González F, Wadhwa S, Rodriguez-Zabala M, et al. *J Med Genet* Epub ahead of print: [please include Day Month Year]. doi:10.1136/jmedgenet-2020-107177

ABSTRACT

Background C-type natriuretic peptide (CNP), its endogenous receptor, natriuretic peptide receptor-B (NPR-B), as well as its downstream mediator, cyclic guanosine monophosphate (cGMP) dependent protein kinase II (cGKII), have been shown to play a pivotal role in chondrogenic differentiation and endochondral bone growth. In humans, biallelic variants in *NPR2*, encoding NPR-B, cause acromesomelic dysplasia, type Maroteaux, while heterozygous variants in *NPR2* (natriuretic peptide receptor 2) and *NPPC* (natriuretic peptide precursor C), encoding CNP, cause milder phenotypes. In contrast, no variants in cGKII, encoded by the protein kinase cGMP-dependent type II gene (*PRKG2*), have been reported in humans to date, although its role in longitudinal growth has been clearly demonstrated in several animal models.

Methods Exome sequencing was performed in two girls with severe short stature due to acromesomelic limb shortening, brachydactyly, mild to moderate platyspondyly and progressively increasing metaphyseal alterations of the long bones. Functional characterisation was undertaken for the identified variants.

Results Two homozygous *PRKG2* variants, a nonsense and a frameshift, were identified. The mutant transcripts are exposed to nonsense-mediated decay and the truncated mutant cGKII proteins, partially or completely lacking the kinase domain, alter the downstream mitogen activation protein kinase signalling pathway by failing to phosphorylate c-Raf 1 at Ser43 and subsequently reduce ERK1/2 activation in response to fibroblast growth factor 2. They also downregulate *COL10A1* and upregulate *COL2A1* expression through SOX9.

Conclusion In conclusion, we have clinically and molecularly characterised a new acromesomelic dysplasia, acromesomelic dysplasia, *PRKG2* type (AMDP).

INTRODUCTION

Longitudinal bone growth is achieved by endochondral ossification in the cartilaginous growth plate. Here, the chondrocytes undergo biochemical and morphological transformation from the resting states, during proliferation and hypertrophy and terminating in their replacement by bone. This process is tightly regulated, requiring a precise

temporal and spatial interaction between hormonal and growth factors.

C-type natriuretic peptide (CNP), its endogenous receptor, natriuretic peptide receptor-B (NPR-B), as well as its downstream mediator, cyclic guanosine monophosphate (cGMP) dependent protein kinase II (cGKII), have been shown to play a pivotal role in chondrogenic differentiation and endochondral bone growth.^{1–3} The binding of CNP to NPR-B leads to synthesis and accumulation of intracellular cGMP that subsequently activates cGKII. In humans, NPR-B and CNP are encoded by the natriuretic peptide receptor 2 (*NPR2*) and natriuretic peptide precursor C (*NPPC*), respectively. Homozygous or compound heterozygous variants in *NPR2* cause acromesomelic dysplasia, type Maroteaux (AMDM (MIM 602875)), a rare autosomal recessive skeletal dysplasia characterised by severe disproportionate short stature, occurring soon after birth with adult height standard deviation score (SDS) < −5, acromesomelic shortening of the extremities, platyspondyly with kyphosis or scoliosis and other dysmorphic features.⁴ Heterozygous *NPR2* variants are associated with a milder phenotype, with short stature, mild mesomelic shortening of the limbs and brachydactyly (MIM 616255) and have also been identified in individuals with idiopathic short stature (ISS).^{5–9} Although the relevance of CNP to skeletal growth has been clearly demonstrated in various animal models,^{10–12} it was only recently that we reported the first heterozygous variants in *NPPC* in humans.¹³ The two loss-of-function CNP variants showed a diminished ability to activate NPR-B and subsequently reduced cGMP synthesis, leading to short stature and small hands.¹³

In contrast, no variants in cGKII, encoded by the protein kinase cGMP dependent type II gene (*PRKG2*), have been reported in humans to date, although its role in longitudinal growth has been demonstrated in several animal models. In 1996, Pfeiffer *et al*¹ were the first to describe the link between cGKII and endochondral ossification, when postnatal dwarfism, cranial alterations and

shortened limbs were unexpectedly observed in *cGKII*^{−/−} mice, later shown to be a consequence of elongated growth plates and impaired chondrocyte hypertrophy.^{1–14} Another model is the Komeda miniature rat Ishikawa (KMI), a naturally occurring homozygous *prkg2* mutant (deletion), which exhibits longitudinal growth retardation starting at 4 weeks after birth and resulting in their limbs being 20%–30% shorter than wild-type (WT) littermates.¹⁵ Dwarfism in American Angus cattle was also found to be due to a homozygous nonsense *PRKG2* mutation, where once again, the mutant cattle were smaller with shorter limbs and metatarsals, fused ulnae and radii and vertebral abnormalities.¹⁶

Here, we report the first homozygous variants in *PRKG2* identified in two unrelated individuals, both with a skeletal dysplasia associated with severe disproportionate short stature due to acromesomelia. We describe the clinical and radiological features observed in these individuals and demonstrate the pathogenic mechanism of the identified variants.

PATIENTS AND METHODS

Proband 1

The proband, a Moroccan girl aged 12 years old, was referred for molecular studies due to severe disproportionate short stature (−4.01 SDS, according to Spanish growth charts, <http://www.aeped.es/noticias/estudios-espanoles-crecimiento-2010>), brachydactyly and mild dysmorphic features. She was the second of three children, born to consanguineous parents (third cousins). Although no birth data were available, at 3 weeks old she had reduced body length (48 cm, −1.93 SDS) and head circumference (35 cm, −0.42 SDS) according to <http://www.aeped.es/noticias/estudios-espanoles-crecimiento-2010>.

She had a congenital complete atrioventricular block (Mobitz IIa) and a pacemaker was implanted at the age of 1 year.

At the age of 10, she presented with a height of 119 cm (−3.21 SDS, <https://www.aeped.es>) and body mass index SDS of 1. She was at Tanner stage 2–3. She had a normal oval-shaped head and no dysmorphic facial features. Physical examination revealed mesomelic shortening of the limbs and short, stubby fingers. Metabolic and hormonal work-up was normal. Both her parents exhibited normal height (mother: 164 cm, −0.01 SDS; father: 165 cm, −1.75 SDS) as did her two brothers. No skeletal abnormalities were observed in any of them. At the age of 12, she had a height of 126 cm (−4.01 SDS). Her sitting height to height ratio was 0.579 (1.21 SDS)¹⁷ and her arm span to height ratio was 0.933. She underwent both femoral and humeral limb lengthening; thus, no further growth data are available. She obtained a final postoperative height of 146 cm (−2.92 SDS) and limb proportionality. She continued to have short, stubby fingers (figure 1F). Her growth curve is shown in online supplemental figure S1.

Radiological analysis of proband 1 at the age of 12 (figure 1) revealed mildly flattening of the thoracic vertebral bodies, mild thoracic scoliosis, lumbar hyperlordosis and short pedicles of the lumbar spine (figure 1A,B). Her lower limbs exhibited mild mesomelic shortening with very mild flaring of the metaphyses and mild genu valgum (C). The growth plate at the knee was prematurely fused (figure 1C). Her radius and ulna were mildly bowed and mild mesomelic shortening was present (figure 1D). She had short broad phalanges and metacarpals (especially the third, fourth and fifth), all of which presented premature fusion



Figure 1 Clinical and radiological phenotype of the two probands. (A–E) Radiographs of proband 1 (female) at the age of 12 years. (F) Hand of proband 1 at the age of 18. (G–M) Radiographs of proband 2 (female) showing the most representative radiological features at different ages (4, 7 and 11 years). At the age of 10, she was at Tanner stage 2–3. Radiological analysis of proband 1 at the age of 12 revealed minimal flattening of the thoracic vertebral bodies. She had thoracolumbar scoliosis and lumbar hyperlordosis (A and B). Lower limbs exhibited mesomelic shortening and broadening of long bones with mild, broadened metaphysis and she had mild genu valgum (C). The growth plates at the knees had already fused. Radius and ulna were mildly bowed and mild mesomelic shortening was present (D). She had short broad phalanges and metacarpals (especially the third and the fifth), all of which were prematurely fused (E and F). Proband 2 at the age of 4 showed moderate platyspondyly with anterior beaking and endplate humps of vertebral borders of dorsolumbar spine (G and H). At the age of 7, her long bones showed widening and irregularities of metaphyseal ends (I), which improved by the age of 11 (J) with widening of the mid-diaphysis of humeri and mild radial bowing at the age of 11 (K). She had short and broad phalanges and metaphyseal irregularity of metacarpals (M, at the age of 11). Radiographs of the evolutionary progress of proband 2 are shown in online supplemental figure 1.

(figure 1E). She had an advanced bone age (+2.6 SDS). The clinical and radiological features were similar to AMDM but with a milder radiological phenotype, no cone-shaped epiphyses in the hands and relatively mild mesomelia.

Proband 2

An Indian girl aged 7 years was first seen in our genetic clinic with a history of short stature and skeletal deformities. She had been referred as a follow-up case of short stature with complaints of gaining little weight since the age of 4 years (height 79 cm, −5.51 SDS, weight 10 kg, −3.61 SDS) according to Indian Academy of Pediatrics (IAP) growth charts (<https://iapindia.org/iap-growth-charts/>). Her upper to lower segment ratio was 1.45 suggestive of disproportionate short stature. She was the second child, born at full term by vaginal delivery, to parents with known consanguinity (third cousins). There was no history of chronic illness in the past or any other relevant medical history. Both parents had short stature according to Centers for Disease Control and Prevention 2000 growth charts (<https://www.cdc.gov/growth-charts/>), mother (147 cm; −2.50 SDS) and father's (158 cm; −2.59 SDS), while her 1-year old brother, at the age of 11.75 years had normal stature (136.7 cm, −1.54 SDS) according to IAP growth charts. No dysmorphic features, brachydactyly or skeletal abnormalities were observed in any of them. The proband, now age 11 years has severe short stature with a height of 102.4 cm (−5.06 SDS), upper to lower segment ratio 1.41 and arm span of 92.7 cm.

Facial dysmorphic features included triangular face with a broad nasal bridge and pointed chin, synophrys, hypertelorism, low set ears. Physical examination revealed generalised hirsutism, prominent costochondral cartilages, sternal prominence, widening of wrists, short stubby fingers, brachydactyly, genu varum and sandal gap. There was no other member in the family with similar clinical features. Routine biochemical evaluation was not significant.

Skeletal surveys were performed at ages 4, 7 and her current age of 11 (figure 1 and online supplemental figure S2). At age 4, moderate platyspondyly with anterior beaking of vertebral borders of dorsolumbar spine was observed (figure 1G,H). Her long bones showed relatively large epiphyses and widening and some irregularity of the metaphyses (online supplemental figure S2). Prominent deltoid tuberosities of the humeri were seen. She had short and broad phalanges and metaphyseal irregularity of metacarpals (online supplemental figure S2) and metatarsals. Her bone age was within normal limits (−1.5 SDS). Her ilia were short with flaring of the iliac wings (online supplemental figure S2). Skeletal survey at 7 years showed increased metaphyseal irregularity of her long bones (figure 1I and online supplemental figure S2). Vertebral alterations were less prominent and restricted to the thoracic region with mild shortening of the pedicles of her lumbar spine (online supplemental figure 1). Her pelvic radiograph showed minor irregularity of the acetabula (Fig S2). The skeletal anomalies were persistent at 11 years old (figure 1J–M and online supplemental figure S2).

Thus, in general, the radiographic hallmarks in both patients include: (1) mild to moderate platyspondyly, (2) moderate brachydactyly, (3) iliac flaring and (4) progressively increasing metaphyseal alterations of the long bones. The overall pattern resembles that of AMDM with a milder phenotype including an absence of cone-shaped epiphyses in the hands.

Genetic analysis

All participants provided informed consent for the performed genetic studies and ethical approval was obtained from the respective institutions. Genomic DNA and RNA was isolated from peripheral blood lymphocytes.

Proband 1

The proband was initially assessed for variants in known skeletal dysplasia genes by using a custom-designed NGS skeletal dysplasia panel (SkeletalSeq.V4, n=327 genes, SeqCap, Roche Nimblegen, Wisconsin, USA). As no causative gene defect was identified, the proband and parents (trio) were subsequently subjected to exome sequencing using Sure Select Human All exon V6 targeted capture (Agilent Technologies, Santa Clara, California, USA), paired-end 150 bp sequencing on a NovaSeq 6000 (Illumina, San Diego, California, USA). Reads were aligned to the hg19 assembly. Variant filtering was performed with the help of VarSeq (Golden Helix, Bozeman, Montana, USA), primarily focusing on mode of inheritance, variants absent in controls (gnomAD), highly conserved nucleotide (GERP++, <http://mendel.stanford.edu/SidowLab/downloads/gerp>) and amino acid (Alamut 2.14, Interactive Biosoftware, France), predicted to be pathogenic by multiple in silico programs: CADD V1.4 (<https://cadd.gs.washington.edu/>), SIFT (<https://sift.bii.a-star.edu.sg/>), Polyphen2 (<http://genetics.bwh.harvard.edu/pph2/>) and Mutation Assessor (<http://mutationassessor.org/r3>). Splice variants were assessed with the aid of Alamut which included MaxEntScan, NNSplice, GeneSplicer and Human Splicing Finder. Non-synonymous or splice site variants were then selected based on first recessive inheritance and then other modes of inheritance and genes associated with Human Phenotype Ontology (HPO) codes. Variants of interest were validated by Sanger sequencing.

Proband 2

Exome sequencing was performed for proband 2 using the Nextera Expanded exome kit (Illumina) and paired-end 100 bp sequencing on a HiSeq2000 (Illumina). The obtained sequencing reads were processed for variant calling using standard pipelines, as previously described.¹⁸ Variant assessment was similar to that previously mentioned. Variants of interest were validated in proband and family by Sanger sequencing.

Genetic screening of *PRKG2*

After the identification of a homozygous variant in *PRKG2* in one proband, *PRKG2* variant screening (NM_006259.2 - exons and intron:exon boundaries) was performed in a cohort of 298 patients with proportionate/disproportionate short stature with or without other skeletal abnormalities by Sanger sequencing. Oligonucleotide sequences for coding regions and intron : exon boundaries are available on request.

Nonsense-mediated decay (NMD) assay

Peripheral blood samples were obtained in ACD (Anticoagulant Citrate Dextrose) buffer vials from probands 1 and 2. Peripheral blood mononuclear cells (PBMCs) were isolated by Ficoll (GE Healthcare, Upsala, Sweden) gradient method. The buffy coat (PBMC-lymphocyte) layer was transferred to a new falcon tube and cells were washed with 1× phosphate-buffered saline (Gibco, Thermo Fisher Scientific, Waltham, Massachusetts, USA) until clearance of the red blood cell ring. Cell viability was verified using trypan blue.

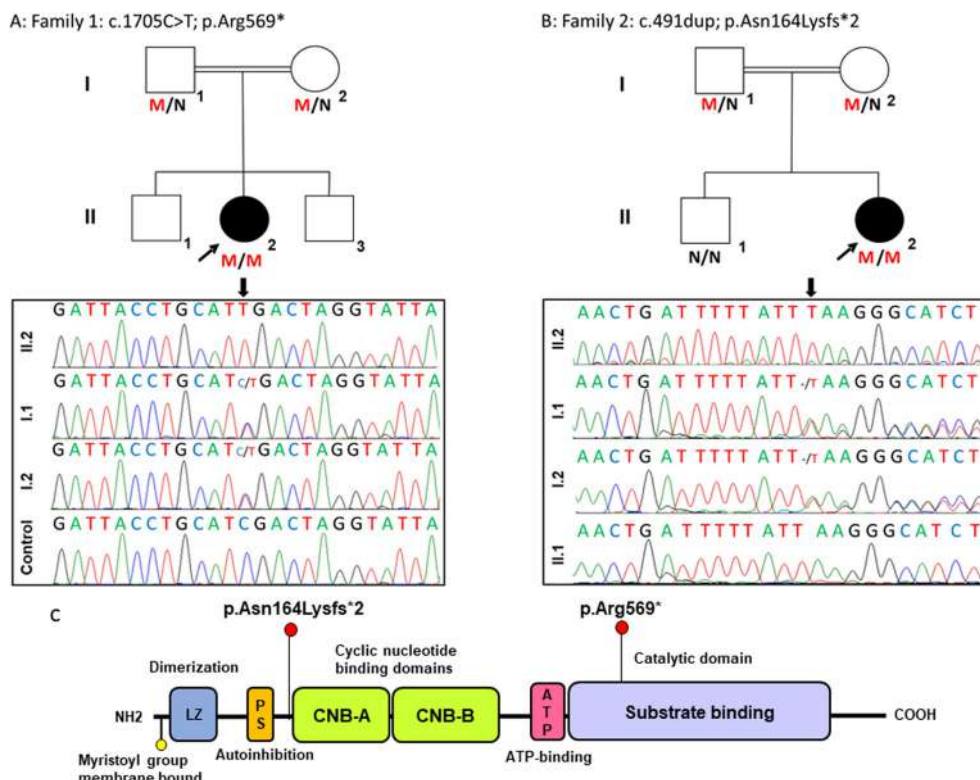


Figure 2 Genetic analysis of families carrying variants in protein kinase cGMP dependent type II gene (*PRKG2*). (A) Pedigree and chromatogram of family 1. Proband is homozygous for the NM_006259.2:c.1705C>T; p.(Arg569*) variant while the parents are heterozygous carriers. (B) Pedigree and chromatogram of family 2. Proband is homozygous for the NM_006259.2:c.491dup; p.(Asn164Lysfs*2) variant, while the parents are heterozygous carriers and the older sibling has a normal genotype. Affected individuals in black symbols. Black arrows mark variant. (C) Structure and functional domains' organisation of cGKII protein, modified from Campbell *et al* (2016)(ref 25), showing the location of the variants identified in the probands. CNB-A/B, cyclic nucleotide-binding sites A and B; LZ, leucine zipper domain; M, mutant; N, normal; NH2 N-terminal; PS, pseudosubstrate.

Cells were then maintained in RPMI-1640 supplemented with 15% fetal bovine serum and 1% antibiotic-antimycotic solution (Gibco, Thermo Fisher Scientific). One hour later, 25 µg/mL cycloheximide (CHX) (Millipore, Darmstadt, Germany) was added to the appropriate wells (treated) and incubated at 37°C, 5% CO₂ and 95% humidity. After 6 hours, treated and untreated cells were harvested and total RNA was isolated using the RNeasy Mini kit (Qiagen, Hilden, Germany) following the manufacturer's recommendations or by the Trizol method. cDNA was generated using the high-capacity cDNA reverse transcription kit (Thermo Fisher Scientific). TaqMan probes for human *PRKG2* (Hs_00922440_m1, Applied Biosystems, Thermo Fisher Scientific) and the endogenous control glyceraldehyde 3-phosphate dehydrogenase (GAPDH) (4326317E, Applied Biosystems, Thermo Fisher Scientific) and the TaqMan Universal PCR Master Mix (Thermo Fisher Scientific) were employed for quantitative real-time PCR, according to manufacturer's instructions.

Plasmid constructions

The empty Myc-DDK-tagged expression pCMV6-Entry plasmid and the human *PRKG2* (NM_006259.2; pCMV6-*PRKG2*-WT) WT plasmid were obtained from Origene Technologies (Rockville, Maryland, USA). *PRKG2* mutants were generated by site-directed mutagenesis of this WT vector according to the manufacturer's instructions (QuikChange Site-Directed Mutagenesis Kit, Agilent Technologies). Mutagenesis primers (mutated base underlined) were the following: 5'-GCTCATTA CAGATGCCCTTAAATAAAAATCAGTTTCTGAAAAG-3'

for the c.491dup; p.Asn164Lysfs*2 (N164Kfs*2) variant, 5'-AGAAGCATTTGATTACCTGCATTGACTAGGTATTATCTA CAGAG-3' for the c.1705C>T; p.Arg569* (R569*) variant and 5'-CCCAGGAAGATAACACGATGACCTGAGGATTGATTTC-3' for the positive control and the American Angus cattle variant, c.2032C>T;p.Arg678* (R678*). All constructs were verified by Sanger sequencing.

Cell culture and transient transfection

HEK293T cells were maintained in 1× Dulbecco's Modified Eagle's Medium (DMEM) supplemented with 10% fetal bovine serum and 1% penicillin/streptomycin (Gibco, ThermoFisher) at 37°C, 5% CO₂ and 95% humidity. Cells were seeded in 6-well plates, and a total of 2 µg of DNA was transfected using jetPRIME (Polyplus-transfection, Illkirch, France) at a 1:2 ratio DNA to jetPRIME reagent following the manufacturer's instructions. In co-transfection studies, equal amount of the two plasmids (1 µg) was added, thus maintaining the 1:2 ratio.

Western blot analysis

Initially we performed dose-dependent experiments using WT *PRKG2* to determine the minimal concentration of fibroblast growth factor 2 (FGF2) and cGMP required to observe reductions in the downstream mitogen activation protein kinase (MAPK) signalling pathway by analysing the expression of phosphorylated extracellular-signal-regulated kinase (ERK) 1/2 by western blot. HEK293T cells were transiently transfected with the empty vector (EV) WT *PRKG2* (pCMV6-*PRKG2*-WT).

Twenty-four hours post-transfection, cells were treated with 100 or 250 μ M of 8-pCPT-cGMP (Sigma Aldrich, Merck, Darmstadt, Germany) for 30 min, followed by the addition of 1 or 2 nM of FGF2 (PeproTech, London, UK) to the appropriate wells for another 30 min to stimulate the MAPK pathway. The cells were then harvested and whole cell protein extract was extracted with the Nuclear Extract Kit (Active Motif, Belgium) according to the manufacturer's instructions. Total protein concentration was determined by Bradford method (Bio-Rad Laboratories, California, USA). Proteins (20 μ g) were resolved under denaturing conditions on a 10% or 12% (for cGKII protein detection) sodium dodecyl sulfate-acrylamide gels and transferred onto nitrocellulose membranes.

Subsequently, to analyse the effect of the two PRKG2 variants, N164Kfs*2 and R569*, on the MAPK signalling pathway, HEK293T cells were transiently transfected with the EV (pCMV6-Myc-DDK), WT PRKG2 (pCMV6-PRKG2-WT), one of the two identified mutants (pCMV6-PRKG2-N164Kfs*2, pCMV6-PRKG2-R569*) or the bovine positive control mutant (pCMV6-PRKG2-R678*). Twenty-four hours post-transfection, cells were treated with 100 μ M of 8-pCPT-cGMP (Sigma-Aldrich, Merck, Darmstadt, Germany) for 30 min, followed by addition of 1 nM of FGF2 (PeproTech, London, UK) to the appropriate wells for another 30 min to stimulate the MAPK pathway. The proteins were extracted as previously described and western blots were undertaken.

The following antibodies were employed: anti-cGKII (1:1000, ab196960; Abcam, Cambridge, UK), phospho-ERK1/2 (1:1000, catalogue no: 9101; Cell Signalling, Leiden, The Netherlands), ERK1/2 (1:1000, catalogue no: 9102; Cell Signalling), phospho-Raf1-Ser43 (1:1000, AP3332a; Abgent, San Diego, California, USA), C-Raf-1 (1:2000, catalogue no: 610152; BD Biosciences, San Jose, California, USA). The proteins were detected using Western Lightning Plus- ECL kit (PerkinElmer, USA). All blots were rehybridised with either GAPDH (1:2000, ab9485; Abcam) or the corresponding non-phosphorylated form of the protein to check for loading variability. Three biological experiments were performed.

Quantification (densitometry) of pMAPK 44/42 levels was performed using the programme ImageJ (<https://imagej.nih.gov/ij/>). Data were normalised to levels of total MAPK (figure 2C).

Quantitative real-time PCR (qPCR)

HEK293T cells were transiently transfected (equal ratio) with combinations of SOX9 and WT or mutant PRKG2 plasmids. EV and the cattle mutant, R678* were employed as negative and positive controls, respectively. Twenty-four hours post-transfection, 250 μ M of 8-pCPT-cGMP (Sigma-Aldrich, Merck) was added to the cells as previously described.¹⁹ Total RNA was isolated 72 hours after treatment using the RNeasy Mini Kit (Qiagen, Hilden, Germany) according to the manufacturer's recommendations. Reverse transcription was performed using the high-capacity cDNA reverse transcription kit (Applied Biosystems, Thermo Fisher Scientific). Expression of collagen type II (COL2A1) and type X (COL10A1), markers of chondrogenic proliferation and hypertrophic differentiation, respectively, was evaluated using TaqMan probes (Hs_00264051 and Hs_00166657, respectively; Applied Biosystems, Thermo Fisher Scientific) and TaqMan Universal PCR Master Mix (Applied Biosystems, Thermo Fisher Scientific). Each plasmid combination was transfected in duplicate, qPCRs were run in triplicate and four biological replicates were performed. The $\Delta\Delta$ CT method was used to determine relative expression levels using RPL13A (Hs_04194366; Applied Biosystems, Thermo Fisher Scientific) as the endogenous control. All data are expressed as percentages compared with the EV.

RESULTS

Genetic analyses

Two homozygous PRKG2 variants, NM_006259.2: c.1705C>T: p.(Arg569*) and c.491dup: p.(Asn164Lysfs*2), were identified in exons 14 and 3, in probands 1 and 2, respectively (figure 3). The variants were confirmed to be present in heterozygosity in their respective parents (figure 3). The frameshift variant is absent from the gnomAD population databases, while the nonsense variant is present in the heterozygous state in one South Asian individual (MAF 0.0033%). The nonsense variant p.(Arg569*) is predicted to produce a truncated protein partially lacking the catalytic domain affecting the substrate-binding region but maintains the regulatory domain, the cyclic nucleotide binding domains, (figure 3) while the frameshift variant p.(Asn164Lysfs*2) is predicted to ablate both the regulatory and catalytic domains (figure 3).

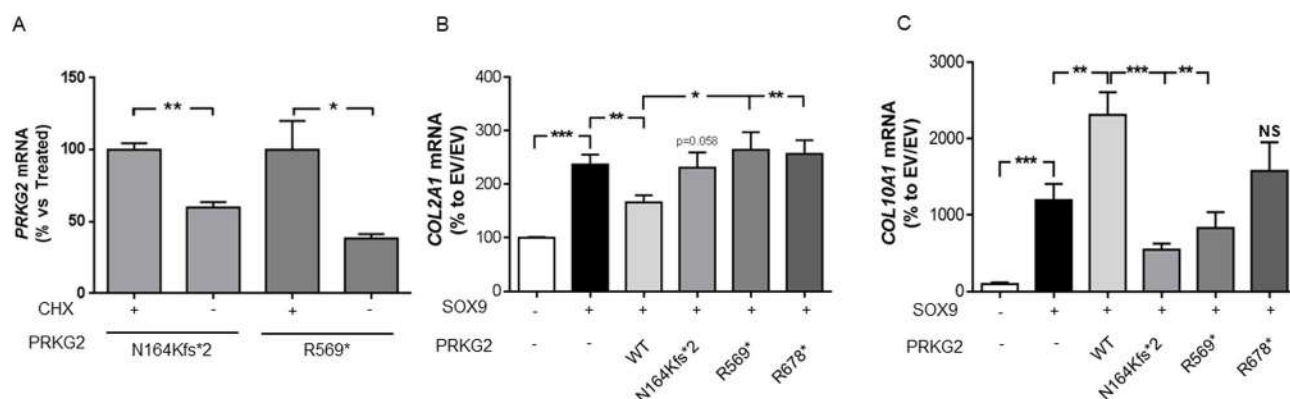


Figure 3 Protein kinase cGMP dependent type II gene (*PRKG2*) variants reduce mRNA expression due to nonsense-mediated decay (NMD) and affect hypertrophic chondrocyte differentiation. (A) NMD assay in probands 1 and 2 peripheral blood mononuclear cells (PBMCs). The mutant *PRKG2* mRNAs are significantly reduced in untreated compared with cycloheximide (CHX)-treated cells, thus demonstrating that the mutant transcripts are exposed to NMD. (B and C) Effects of both *PRKG2* variants on *COL2A1* (B) and *COL10A1* (C) expression determined by real-time quantitative PCR in HEK293T cells. *PRKG2* variants are unable to downregulate *COL2A1* and upregulate *COL10A1* mRNA levels, respectively, compared with wild type (WT). Data are presented as percentages relative to empty vector (EV)/EV. Significant p values in the Student's t-test are indicated with asterisks (* $p<0.05$, ** $p<0.01$, *** $p<0.001$), NS signifies no significant results.

A summary of the exome sequencing data is provided in online supplemental data. A list of all homozygous variants detected in probands 1 and 2 are presented in online supplemental tables S1 and S2, respectively.

Functional studies

PRKG2 variants lead to reduced mRNA expression in proband PBMCs

As both variants were predicted to result in prematurely truncated proteins, we assessed whether the mutant mRNA was subjected to NMD using PBMCs from the patients in the presence or absence of NMD inhibitor, CHX. *PRKG2* expression was significantly increased in the treated compared with untreated cells for both variants (c.491dup; p.(Asn164Lysfs*2), $p < 0.01$ and c.1705C>T; p.(Arg569*), $p < 0.05$), thus confirming that NMD occurs for both variants (figure 4A).

PRKG2 mutants are unable to downregulate MAPK signalling

First, we investigated whether the variants affected the synthesis of cGKII by performing western blot analysis of HEK293T cell lysates transfected with WT or mutant *PRKG2*. All truncated mutant proteins were detected, although their expression levels were reduced compared with WT (figure 2A).

Second, we determined whether the cGKII mutants were able to inhibit the FGF-induced MAPK pathway by transiently transfecting HEK293T cells with WT or mutant *PRKG2* and treated with a cGMP analogue (8 pCPT-cGMP) and FGF2 to stimulate the MAPK pathway. We analysed their ability to phosphorylate Raf-1 at Ser-43 and ERK1/2. FGF2 was unable to induce phosphorylation of Raf-1 at Ser-43 per se, but phosphorylated ERK1/2 in the absence of 8 pCPT-cGMP, as previously described.²⁰ WT *PRKG2*/cGKII phosphorylated Raf-1 and reduced FGF2-induced ERK1/2 phosphorylation in a cGMP-dependent manner. However, all mutants significantly failed to phosphorylate Raf-1 at Ser-43 and thus did not reduce ERK1/2 phosphorylation induced by FGF2 (figure 2B,C).

PRKG2 mutants uncouple the switch from proliferative to hypertrophic differentiation through impaired *SOX9* function

To investigate the effect of *PRKG2* variants in the regulation of proliferation and hypertrophic differentiation of chondrocytes by *SOX9*, expression of *COL2A1* and *COL10A1*, markers of chondrocyte differentiation and hypertrophy, respectively, was determined by qPCR. Cells transfected with *SOX9* showed a twofold increase in *COL2A1* expression compared with the EV control (237 ± 18.4 , $p < 0.001$; figure 4B). Cotransfection with WT *PRKG2* significantly reduced *SOX9*-induced *COL2A1* levels ($p < 0.01$) in HEK293T cells. In contrast, neither of the *PRKG2* mutants were able to suppress *COL2A1* expression (N164Kfs*2, $p = 0.058$; R569*, $p < 0.05$; R678*, $p < 0.01$; figure 4B). Cotransfection with WT *PRKG2* revealed a twofold increase in *COL10A1* expression compared with *SOX9*-transfected cells ($p < 0.01$) (figure 4C). Both human *PRKG2* variants, N164Kfs*2 and R569*, failed to restore *COL10A1* expression to WT *PRKG2* (N164Kfs*2, $p < 0.0001$; R569*, $p < 0.01$). However, the bovine mutant R678* did not reduce *COL10A1* expression, unlike the two human mutants, as previously described (figure 4C).¹⁶

DISCUSSION

In this study, two homozygous loss-of-function variants in *PRKG2* were identified in two individuals with an acromesomelic skeletal

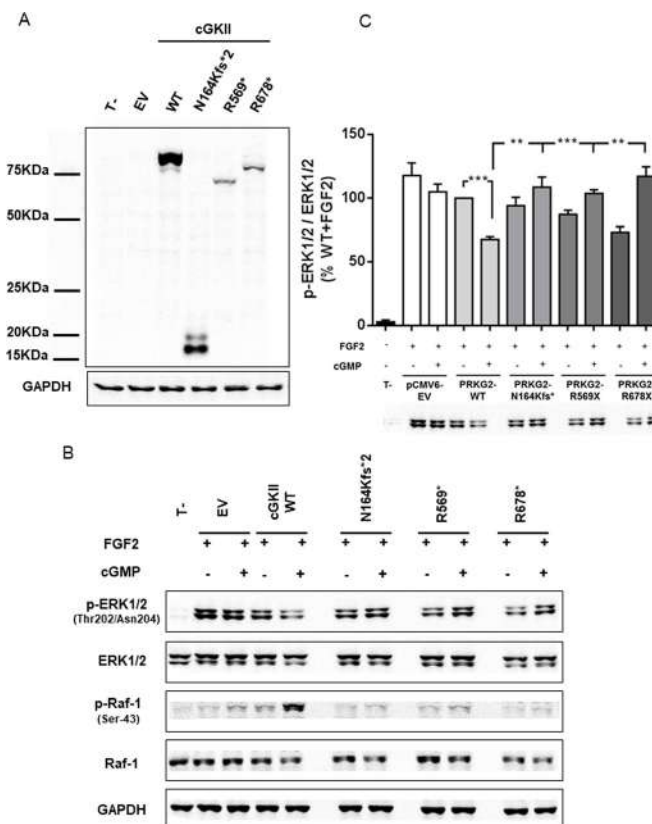


Figure 4 Protein kinase cGMP dependent type II gene (*PRKG2*) mutants affect cyclic guanosine monophosphate (cGMP) dependent protein kinase II (cGKII) protein synthesis and reduce its function. (A) Western blot analysis of wild-type (WT) and *PRKG2* mutants using anti-cGKII antibody and protein loading control with anti-GAPDH antibody. The two human *PRKG2* mutants and the bovine positive control mutant lead, as expected, to shortened cGKII proteins. The expected size of the mutated proteins, N164Kfs*2: 18.5 kDa, R569*: 65.1 kDa and R678*: 77.6 kDa, was calculated by using the ExPaSy online tool (<https://web.expasy.org>). The N164Kfs*2 mutant revealed two bands, with the stronger lower band being of the expected size. No experiments were performed to determine what the larger weaker band may be but possible reasons could be alternative translation to that predicted or due to post-translational modification. (B) Effect of *PRKG2* mutants on the regulation of the fibroblast growth factor 2 (FGF2) induced mitogen activation protein kinase (MAPK) pathway using western blot of phosphorylated Raf-1 and ERK1/2 proteins showing that neither human *PRKG2* mutants nor the positive control bovine mutant are able to downregulate ERK activation compared with WT in the presence of 8-pCPT-cGMP in HEK293 cells. Protein loading control using anti-GAPDH antibody. (C) Quantification of the pMAPK 44/42 proteins by western blot densitometry showing that the two human *PRKG2* mutants and the bovine mutant are significantly unable to downregulate FGF2-induced ERK1/2 phosphorylation compared with WT in the presence of 8-pCPT-cGMP in HEK293 cells. Three biological experiments were performed, and significance values are represented as * $p < 0.05$, ** $p < 0.01$ and *** $p < 0.001$. EV, empty vector; FGF2, fibroblast growth factor 2; GAPDH, glyceraldehyde 3-phosphate dehydrogenase; T-, untransfected cells.

dysplasia. No other *PRKG2* variants were found in the screening of 298 individuals with proportionate/disproportionate short stature with or without other skeletal abnormalities.

The two girls have severe disproportionate short stature with acromesomelic shortening of the limbs and mild to moderate platyspondyly. Metaphyseal dysplasia of the long bones was

Table 1 Comparison of the clinical, genetic and radiological features of the different types of acromesomelic dysplasias including the new acromesomelic dysplasia PRKG2 type (AMDP)

| Features | Acromesomelic dysplasia, type Maroteaux (AMDM) | Grebe dysplasia* | Fibular hypoplasia and complex brachydactyly (Du Pan syndrome) | Acromesomelic dysplasia, Osebold-Resmondini type† | Acromesomelic dysplasia, PRKG2 type (AMDP) | |
|---------------------------------|---|---|--|---|---|--|
| OMIM | 602875 | 200700, 609441, 201250, 603248 | 228900 | 112910 | — | |
| Gene (inheritance) | <i>NPR2</i> (AR) | <i>GDF5</i> , <i>BMPR1B</i> (AR) | <i>GDF5</i> , <i>BMPR1B</i> (AR) | — (AD) | <i>PRKG2</i> (P1) (AR) | <i>PRKG2</i> (P2) (AR) |
| Short stature | + (severe) | + (severe) | —/+ (moderate) | + (moderate) | + (severe) | + (severe) |
| Adult height (cm) | 95–122 | 100–140 | ND | 135–160 | 130 (Est) | NR |
| Acromesomelia | ++ | + | + | + | + | + |
| Bowed forearm | + | + | — | + | + | +/- |
| Brachydactyly | + | + | + | + | + | + |
| Hand phalanges (hypoplasia) | + | + | + | +(second) (3rd–5th syndactyly) | + | + |
| Hyperlordosis | + | — | — | — | + | — |
| Talipes equinovarus | — | + | + | + | — | — |
| Toes | Long broad halluces | Hypoplasia (non-functional) | Hypoplasia (knob-like) | Short, broad, sandal gap | Normal | Short, broad, sandal gap |
| Nail aplasia/hypoplasia | + | — | + | — | — | — |
| Facial dysmorphism | Frontal bossing, depressed nasal ridge, short nose | — | — | — | — | Triangular face, broad nasal bridge, pointed chin, synophrys, hypertelorism and low set ears |
| Other features | — | Hypoplastic uterus, absent ovaries§ | — | — | — | Hirsutism |
| Prenatal presentation | — | +/- | ND | + | ND | ND |
| Phenotype in heterozygous state | Short stature, brachydactyly, mild clinical features | Brachydactyly | — | NA | — | Short stature? |
| Radiological features | | | | | | |
| Skull | Large, with frontal bossing | Normal | Normal | Normal | Normal | |
| Spine | <ul style="list-style-type: none"> ▶ Oval-shaped vertebrae in infancy ▶ Ventral protrusion of centrally located 'tongue' ▶ Posterior wedging of vertebrae ▶ Short pedicles | Normal | Normal | Normal | 1. Short pedicles 2. Anterior beaking vertebral bodies of thoracolumbar junction | |
| Pelvis | <ul style="list-style-type: none"> ▶ Acetabular notch ▶ Relative hypoplasia of base of ilia | Normal | Normal | Normal | Mild acetabular irregularity | |
| Long tubular bones | <ul style="list-style-type: none"> ▶ Mesomelia (+++) with upper limbs more severely affected than lower limbs ▶ Bowed radius ▶ Dislocation/subluxation of radial head ▶ Flared metaphyses | <ul style="list-style-type: none"> ▶ Mesomelia (++) with relatively normal rhizomelic segments | <ul style="list-style-type: none"> ▶ Absent/hypoplastic fibulae ▶ Dislocated knees | 1. Mesomelia (++/+++) | ▶ Mesomelia (+) ▶ Mildly bowed radius and ulna ▶ Relatively large epiphyses ▶ Metaphyseal irregularity | |

Continued

Developmental defects

Table 1 Continued

| Features | Acromesomelic dysplasia, type Maroteaux (AMDM) | Grebe dysplasia* | Fibular hypoplasia and complex brachydactyly (Du Pan syndrome) | Acromesomelic dysplasia, Osebold-Resmondini type† | Acromesomelic dysplasia, PRKG2 type (AMDP) |
|---------------------|--|--|--|--|--|
| Short tubular bones | <ul style="list-style-type: none"> ▶ Brachydactyly (+++) with relative sparing of big toes ▶ Cone-shaped epiphyses with premature fusion | <ul style="list-style-type: none"> ▶ Brachydactyly (++/+++) ▶ Carpal/tarsal fusions ▶ Absent ossification metacarpals, metatarsals, some carpal and tarsal bones and proximal and middle phalanges ▶ Postaxial polydactyly | <ul style="list-style-type: none"> ▶ Brachydactyly (++/+++) ▶ Carpal/tarsal fusions ▶ Absent ossification metacarpals, metatarsals, some carpal and tarsal bones and proximal and middle phalanges ▶ Postaxial polydactyly | <ul style="list-style-type: none"> ▶ Brachydactyly (++/+++) ▶ Hypoplastic/absent ossification of middle phalanges of hands and feet ▶ Phalangeal synostosis ▶ Carpal and tarsal synostosis ▶ Bipartite calcanei | <ul style="list-style-type: none"> ▶ Brachydactyly (+) ▶ Advanced bone age ▶ Premature fusion of epiphyses of hands and knees |

*Grebe dysplasia encompassing also Hunter-Thompson dysplasia and acromesomelic dysplasia with genital anomalies (Demirhan type).

†One family described.³⁶

‡Appears between 1 and 2 years of age.

§Described in acromesomelic dysplasia with genital anomalies (Demirhan type).

NA, not applicable as AD inheritance; ND, not described; NR, not reached adult height.

present in both probands, although in proband 2, this was not evident in early childhood but was most noted at the age of 7. The skeletal anomalies are similar to those observed in AMDM, although the platyspondyly and brachydactyly appears to be milder, as is the mesomelic shortening, and to a greater degree in proband 1 compared with proband 2. The identification of further cases will enable us to determine if indeed this is a milder phenotype or whether there is a broad phenotypic spectrum. These clinical and radiological similarities are logical since AMDM is caused by biallelic variants in the gene encoding NPR-B, the main receptor for CNP and is located just upstream from cGKII.

The importance of CNP/NPR-B signalling in the skeletal human growth has been widely demonstrated as variants in NPR-B and CNP have been associated with various skeletal dysplasias and growth disorders. Common phenotypic features such as short stature and brachydactyly are observed but the severity is variable, principally depending on the mode of inheritance but also due to other factors such as polymorphisms in modifying genes, the majority of which remain unknown, epigenetics, diet and so on. The most severe phenotype is observed in AMDM individuals with homozygous *NPR2* variants, whereas the phenotype is milder in some heterozygous affected individuals with only isolated short stature, and even individuals may be asymptomatic.^{5 21}

While no pathogenic variants in human *PRKG2* have been reported until this study, its role in skeletal growth has been widely supported by animal models such as cGKII null mice, KMI rat with a *Prkg2* deletion and American Angus cattle with the nonsense mutation (p.Arg678*), all of which developed growth retardation with shortened limbs (>30%) and trunk, soon after birth.^{1 14 16 19} The shortened limbs and radiological features are similar to those observed in the two probands.

As both *PRKG2* variants, c.491dup; p.(Asn164Lysfs*2) in exon 3 and c.1705C>T: p.(Arg569*) in exon 14, are predicted to cause premature truncations of cGKII, we investigated if the transcripts were exposed to NMD. Using lymphocyte cells from the patients, both mutant transcripts were degraded or partially degraded by NMD. This is in contrast to that observed for the bovine mutant located in exon 16, c.2032C>T; p.Arg678* which was not found to be degraded by NMD.¹⁶ However,

using in silico predictions, both the human and bovine nonsense variants may be exposed to NMD while the frameshift variant was not thus, the location of the mutants along the 19 exons of *PRKG2* does not appear to explain these results. In addition, due to the lack of tissue availability, we cannot demonstrate that our findings in lymphocytes can be representative of what is occurring in the chondrocytes. Tissue-specific NMD has been shown in various disorders including in Schmid metaphyseal dysplasia (MIM 156500), where NMD was shown to be specific to cartilage and did not occur in the non-cartilage lymphoblast or bone cells.²²

We were also able to observe the truncated mutant proteins by western analysis. Moreover, the mutant proteins showed a reduced expression in vitro compared with WT (figure 2A). Taken together, these results provide evidence that NMD reduces the amount of mRNA transcribed from the alleles carrying the p.As164Lysfs*2 and p.Arg569* variants, hence preventing or reducing the synthesis of abnormal cGKII protein.

The protein cGKII is a 762-amino acid enzyme that belongs to the serine/threonine protein kinase family. It consists of three distinctive domains: an amino-terminal (N), a regulatory (R) and a carboxy-terminal catalytic domain (C) (figure 3C). The N-terminus has been shown to be involved in dimerisation, autoinhibition of the catalytic activity and cellular localisation of the protein to the cell membrane.^{23 24} The regulatory domain has two cyclic nucleotide-binding sites in tandem (CNB-A and CNB-B) that exhibit different affinities for cGMP binding (CNB-B > CNB-A).²⁵ Finally, the C-terminal domain or active domain contains ATP and substrate-binding sites necessary for phosphorylation of consensus sequences on target proteins.²⁶ Both *PRKG2* variants lack the catalytic domain and thus have no kinase activity. Moreover, the p.(Asn164Lysfs*2) mutant also lacks the regulatory domain, which would mean that it is also unable to bind cGMP, necessary for the activation of the enzyme. Therefore, the p.(Arg569*) and p.(Asn164Lysfs*2) variants are likely to be abnormal and catalytically inactive proteins.

To demonstrate this, we examined their ability to downregulate the MAPK pathway in vitro. CNP promotes chondrocyte proliferation by antagonising FGF-induced MAPK signalling in the growth plate.²⁷ Activation of fibroblast growth factor receptor-3 (FGFR3)-MAPK pathway (FGFR3/Ras/Raf/MEK/ERK) by FGFs

is the underlying mechanism of the chondrocyte growth arrest observed in various skeletal dysplasias and growth disorder such as achondroplasia (MIM 100800).^{27,28} Conversely, activation of cGKII, by CNP-mediated intracellular elevation of cGMP, has been reported to inhibit FGF-induced MEK and ERK1/2 phosphorylation in fibroblasts and tibia explants thus restoring and promoting chondrocyte proliferation in the growth plate.^{29,30} Moreover, chemical inhibition of FGFR3 and MEK1/2 rescued FGF2-induced growth arrest in vitro^{25,27} and overexpression of CNP in the cartilage growth plate prevented dwarfism in a mouse model of achondroplasia by attenuating ERK1/2 activation.³⁰ Both *PRKG2* human mutants, R569* and N164Kfs*2, as well as the bovine R678* mutant, failed to inhibit FGF2-induced ERK1/2 phosphorylation in the presence of the cGMP analogue, 8-pCPT-cGMP, previously shown to downregulate ERK1/2 activation.²⁰ Moreover, we also investigated whether the *PRKG2* mutants were able to phosphorylate Raf-1 at Serine 43, necessary for the cGKII inhibitory effect on FGF-induced MAP kinase activation. Neither of the two mutants were able to phosphorylate and thus inactivate Raf-1 at Ser-43 and consequently reduce ERK activation. Therefore, these data confirm that both variants are unable to abolish MAPK cascade activation in response to FGF2, thus leading to growth retardation.

Based on previous studies in the KMI rat with a *Prkg2* deletion, cGKII was shown to act as a molecular switch by impeding the translocation of SOX9 to the nucleus and thus attenuating its ability to induce chondrocyte differentiation, impeding both chondrocyte proliferation and conversion of proliferating chondrocytes into hypertrophic chondrocytes.¹⁹ Both R569* and N164Kfs*2 *PRKG2* mutants showed increased expression of *COL2A1*, a marker of chondrocyte proliferation, and decreased expression of *COL10A1*, a marker of hypertrophy, compared with WT in HEK293T cells. These results are consistent with those observed in chondrocyte primary cultures from KMI rats tibia and in ATDC5 and HuH-7 cell lines transfected with cGKII mutant lacking kinase domain.¹⁹ However, the bovine R678* mutant increased *COL2A1* expression but did not significantly decrease *COL10A1* expression, duplicating the result observed by Koltes *et al*¹⁶ who postulated that these differences may be due to tissue collection or sample source as they evaluated expression levels in bovine growth plate cartilage. However, in this current study, we analysed all three mutants using the in vitro cell culture method described by Chikuda *et al*.¹⁹ Despite discrepant results of *COL10A1* expression in the investigations of *PRKG2* mutants and no proof of what is occurring in the growth plate, it is tempting to speculate that aberration of type X collagen expression would interfere with terminal maturation of chondrocytes and thus the metaphyseal abnormalities observed in the probands.

Interestingly, although *Prkg2*^{-/-} animal models showed similar growth restraint phenotypes to those observed in *Npr2* and *Nppc* mice models,^{10,31} the histology of the growth plate is quite different. Conversely to *Npr2*^{-/-} and *Nppc*^{-/-} mice that exhibited shorter growth plates but regular organisation of chondrocyte zones, the elongated growth plate of *Prkg2*^{-/-} mice and rats maintained an organised pattern but revealed an intermediate layer between the proliferative and hypertrophic zones, where chondrocytes had ceased proliferation but had failed to start hypertrophic differentiation. However, the Angus cattle dwarf growth plate showed a general loss of organisation but once again, mixing of proliferative and hypertrophic chondrocytes.¹⁶

GKII is not only implicated in growth but has also been shown to play a role in other pathways including gastrointestinal secretion of chloride and water via phosphorylation of CFTR (cystic

fibrosis transmembrane conductance regulator protein)^{1,32} and might also regulate aldosterone secretion and blood pressure³³ although the latter appears to be due to overexpression of cGKII rather than loss.³⁴ In addition, these systems may be regulated by GKII due to NPR-A activation in response to CNP rather than via NPR-B. The clinical features observed in both probands seem to be at present restricted to the skeletal system.

In the current nosology of skeletal dysplasias, there are four acromesomelic dysplasias (Group 16³⁵): the three autosomal recessively inherited dysplasias, AMDM caused by variants in *NPR2* (MIM 6002875); Grebe dysplasia (MIM 200700, 609441) encompassing also Hunter-Thompson dysplasia (MIM 201250) and acromesomelic dysplasia with genital anomalies (Demirhan type (MIM 603248)) caused by variants in *GDF5* and *BMPR1B*; fibular hypoplasia and complex brachydactyly (Du pan dysplasia (MIM 228900)) also caused by variants in *GDF5* and *BMPR1B* and lastly acromesomelic dysplasia Osebold-Remondini type (MIM 112910) in which the molecular defect has not been identified and has only been reported in one multigenerational family.³⁶ The clinical and radiological similarities and differences of the various forms in comparison with the new entity, acromesomelic dysplasia *PRKG2* type, are summarised in table 1.

We investigated whether heterozygous carriers of *PRKG2* variants are unaffected or have a milder phenotype, similar to that observed in some heterozygotes of *NPR2*, *GDF5* and *BMPR1B* variants (MIM 616255, 615072, 112600, 113100, 610017, 615298, 616849), genes implicated in other acromesomelic dysplasias. The parents of proband 1 have normal stature, although the father's height is at the lower end (−1.75 SDS), while the parents of proband 2 both have short stature (mother −2.50 SDS, father −2.59 SDS). All four do not have any skeletal or dysmorphic features. Thus, at present we cannot conclude if heterozygous *PRKG2* variants have an influence on height. The identification of further cases will be necessary to determine this.

At present, no therapies are available for children with *PRKG2* variants. Currently, there are various clinical trials being undertaken or completed in children with achondroplasia including: CNP analogues (Vosoritide (BMN111), BioMarin, California, USA³⁷; TransCon CNP, Ascendis Pharma, Denmark,³⁸ soluble FGFR3 (TA-46; Pfizer, California, USA)³⁹ and FGFR3 selective tyrosine kinase inhibitors (infigratinib, compound BGJ398; QED Therapeutics, California, USA).⁴⁰ The CNP analogues would not be able to repress the activation of the MAPK pathway by the *PRKG2* mutants but soluble FGFR3 or FGFR selective tyrosine kinase inhibitors may be able to counteract this activation.

In conclusion, we describe a new skeletal dysplasia caused by biallelic variants in *PRKG2*. The inability to downregulate MAPK signalling as well as modulate SOX9 actions confirms the pathogenicity of the two identified variants. We suggest the naming of this new acromesomelic dysplasia as acromesomelic dysplasia, *PRKG2* type (AMDP).

Author affiliations

¹Institute of Medical and Molecular Genetics (INGEMM), IdiPAZ, Hospital Universitario La Paz, UAM, Madrid, Spain

²Skeletal Dysplasia Multidisciplinary Unit (UMDE) and ERN-BOND, Hospital Universitario La Paz, Madrid, Spain

³Genomics and Molecular Medicine Division, CSIR—Institute of Genomics and Integrative Biology, New Delhi, India

⁴CIBERER, ISCIII, Madrid, Spain

⁵Dept. of Pediatrics, Maulana Azad Medical College and Lok Nayak Hospital, New Delhi, India

⁶Dept. of Pediatrics, Hospital Universitario Infanta Leonor, Madrid, Spain

⁷Dept. of Pediatrics, Universidad Complutense de Madrid, Madrid, Spain

⁸Dept. of Pediatric Endocrinology, Hospital Universitario Ramon y Cajal, Madrid, Spain

⁹Center for Intractable Disease, Saitama Medical University Hospital, Saitama, Japan
¹⁰Academic Unit of Child Health, The University of Sheffield, Sheffield, UK
¹¹Dept. of Radiology and ERN-BOND, Sheffield Children's Hospital NHS Foundation Trust, Sheffield, UK

Correction notice The article has been corrected since it was published online first. The caption of figures 2, 3 and 4 were incorrectly ordered; they have been amended.

Acknowledgements We wish to thank the patients and families for their help during this study.

Contributors KEH and MF established and obtained financing of the project. SKU, LS-M, MA-B, MBR-M, HS, SKo clinically diagnosed and followed up the patients. GN and ACO examined and reported the radiological data. SW, MR-Z, MA-C, IA, SZ, DK, NK, US, MF and KEH analysed genetic data. FD-G, SW, IH, MR-Z, MA-C performed functional characterisation. KEH and MF analysed the data and supervised the project. FD-G and KEH wrote the first draft of the manuscript, tables and figures. All the authors revised the manuscript and approved the final version.

Funding This work was supported in part by the following grants: SAF2017-84646-R from MINECO (to KEH), Council of Scientific & Industrial Research (CSIR), India (to MF) and Indian Council of Medical Research (to MF). FG-D was supported by an FPU studentship from the Spanish Ministry of Education.

Competing interests None declared.

Patient consent for publication Obtained.

Ethics approval Ethical approval was obtained from Hospital Universitario La Paz, Madrid, Spain, and CSIR—Institute of Genomics and Integrative Biology, New Delhi, India. All participants provided informed consent for the performed genetic studies. All the procedures were performed under the Declaration of Helsinki and relevant policies in Spain and India.

Provenance and peer review Not commissioned; externally peer reviewed.

Data availability statement Data are available on reasonable request. All data relevant to the study are included in the article or uploaded as supplementary information.

Supplemental material This content has been supplied by the author(s). It has not been vetted by BMJ Publishing Group Limited (BMJ) and may not have been peer-reviewed. Any opinions or recommendations discussed are solely those of the author(s) and are not endorsed by BMJ. BMJ disclaims all liability and responsibility arising from any reliance placed on the content. Where the content includes any translated material, BMJ does not warrant the accuracy and reliability of the translations (including but not limited to local regulations, clinical guidelines, terminology, drug names and drug dosages), and is not responsible for any error and/or omissions arising from translation and adaptation or otherwise.

ORCID iDs

Amaka C Offiah <http://orcid.org/0000-0001-8991-5036>
 Karen E. Heath <http://orcid.org/0000-0002-5816-7044>

REFERENCES

- Pfeifer A, Aszodi A, Seidler U, Ruth P, Hofmann F, Fässler R. Intestinal secretory defects and dwarfism in mice lacking cGMP-dependent protein kinase II. *Science* 1996;274:2082–6.
- Yasoda A, Ogawa Y, Suda M, Tamura N, Mori K, Sakuma Y, Chusho H, Shiota K, Tanaka K, Nakao K. Natriuretic peptide regulation of endochondral ossification. Evidence for possible roles of the C-type natriuretic peptide/guanylyl cyclase-B pathway. *J Biol Chem* 1998;273:11695–700.
- Krejci P, Masri B, Fontaine V, Mekikian PB, Weis M, Prats H, Wilcox WR. Interaction of fibroblast growth factor and C-natriuretic peptide signaling in regulation of chondrocyte proliferation and extracellular matrix homeostasis. *J Cell Sci* 2005;118:5089–100.
- Bartels CF, Bükümmez H, Padayatti P, Rhee DK, van Ravenswaaij-Arts C, Pauli RM, Mundlos S, Chitayat D, Shih L-Y, Al-Gazali LI, Kant S, Cole T, Morton J, Cormier-Daire V, Faivre L, Lees M, Kirk J, Mortier GR, Leroy J, Zabel B, Kim CA, Crow Y, Braverman NE, van den Akker F, Warman ML. Mutations in the transmembrane natriuretic peptide receptor NPR-B impair skeletal growth and cause acromesomelic dysplasia, type Maroteaux. *Am J Hum Genet* 2004;75:27–34.
- Olney RC, Bükümmez H, Bartels CF, Prickett TCR, Espiner EA, Potter LR, Warman ML. Heterozygous mutations in natriuretic peptide receptor-B (NPR2) are associated with short stature. *J Clin Endocrinol Metab* 2006;91:1229–32.
- Vasques GA, Amano N, Docko AJ, Funari MFA, Quedas EPS, Nishi MY, Arnhold IJP, Hasegawa T, Jorge AAL. Heterozygous mutations in natriuretic peptide receptor-B (NPR2) gene as a cause of short stature in patients initially classified as idiopathic short stature. *J Clin Endocrinol Metab* 2013;98:E1636–44.
- Amano N, Mukai T, Ito Y, Narumi S, Tanaka T, Yokoya S, Ogata T, Hasegawa T. Identification and functional characterization of two novel NPR2 mutations in Japanese patients with short stature. *J Clin Endocrinol Metab* 2014;99:E713–8.
- Wang SR, Jacobsen CM, Carmichael H, Edmund AB, Robinson JW, Olney RC, Miller TC, Moon JE, Mericq V, Potter LR, Warman ML, Hirschhorn JN, Dauber A. Heterozygous mutations in natriuretic peptide receptor-B (NPR2) gene as a cause of short stature. *Hum Mutat* 2015;36:474–81.
- Hisado-Oliva A, Garre-Vázquez AI, Santaolalla-Caballero F, Belinchón A, Barreda-Bonis AC, Vasques GA, Ramirez J, Luzuriaga C, Carlone G, González-Casado I, Benito-Sanz S, Jorge AA, Campos-Barros A, Heath KE. Heterozygous NPR2 mutations cause disproportionate short stature, similar to Léri-Weill dyschondrosteosis. *J Clin Endocrinol Metab* 2015;100:E1133–42.
- Chusho H, Tamura N, Ogawa Y, Yasoda A, Suda M, Miyazawa T, Nakamura K, Nakao K, Kurihara T, Komatsu Y, Itoh H, Tanaka K, Saito Y, Katsuki M, Nakao K. Dwarfism and early death in mice lacking C-type natriuretic peptide. *Proc Natl Acad Sci U S A* 2001;98:4016–21.
- Jiao Y, Yan J, Jiao F, Yang H, Donahue LR, Li X, Roe BA, Stuart J, Gu W. A single nucleotide mutation in Nppc is associated with a long bone abnormality in lbab mice. *BMC Genet* 2007;8:16.
- Tsuji T, Kondo E, Yasoda A, Inamoto M, Kiyosu C, Nakao K, Kunieda T. Hypomorphic mutation in mouse Nppc gene causes retarded bone growth due to impaired endochondral ossification. *Biochem Biophys Res Commun* 2008;376:186–90.
- Hisado-Oliva A, Ruzafa-Martin A, Sentchordi L, Funari MFA, Bezanilla-López C, Alonso-Bernáldez M, Barraza-García J, Rodríguez-Zabala M, Lerario AM, Benito-Sanz S, Aza-Carmona M, Campos-Barros A, Jorge AAL, Heath KE. Mutations in C-natriuretic peptide (Nppc): a novel cause of autosomal dominant short stature. *Genet Med* 2018;20:91–7.
- Kawasaki Y, Kugimiya F, Chikuda H, Kamekura S, Ikeda T, Kawamura N, Saito T, Shinoda Y, Higashikawa A, Yano F, Ogasawara T, Ogata N, Hoshi K, Hofmann F, Woodgett JR, Nakamura K, Chung U-il, Kawaguchi H. Phosphorylation of GSK-3beta by cGMP-dependent protein kinase II promotes hypertrophic differentiation of murine chondrocytes. *J Clin Invest* 2008;118:2986–15.
- Tsuchida A, Yokoi N, Namae M, Fuse M, Masuyama T, Sasaki M, Kawazu S, Komeda K. Phenotypic characterization of the Komeda miniature rat Ishikawa, an animal model of dwarfism caused by a mutation in Prkg2. *Comp Med* 2008;58:560–7.
- Koltes JE, Mishra BP, Kumar D, Kataria RS, Totir LR, Fernando RL, Cobbold R, Steffen D, Coppieters W, Georges M, Reecy JM. A nonsense mutation in cGMP-dependent type II protein kinase (PRKG2) causes dwarfism in American Angus cattle. *Proc Natl Acad Sci U S A* 2009;106:19250–5.
- Arriba Muñoz A, Domínguez Cajal M, Rueda Caballero C, Labarta Aizpún JL, Mayayo Dehesa E, Ferrández Longás A. Sitting height/standing height ratio in a Spanish population from birth to adulthood (“Relación talla sentada/talla de pie del nacimiento a la adultez en niños españoles”). *Arch Argent Pediatr* 2013;111:309–14.
- Faruq M, Narang A, Kumari R, Pandey R, Garg A, Behari M, Dash D, Srivastava AK, Mukerji M. Novel mutations in typical and atypical genetic loci through exome sequencing in autosomal recessive cerebellar ataxia families. *Clin Genet* 2014;86:335–41.
- Chikuda H, Kugimiya F, Hoshi K, Ikeda T, Ogasawara T, Shimoaka T, Kawano H, Kamekura S, Tsuchida A, Yokoi N, Nakamura K, Komeda K, Chung U-I, Kawaguchi H. Cyclic GMP-dependent protein kinase II is a molecular switch from proliferation to hypertrophic differentiation of chondrocytes. *Genes Dev* 2004;18:2418–29.
- Kamemura N, Murakami S, Komatsu H, Sawano M, Miyamoto K, Ishidoh K, Kishimoto K, Tsuji A, Yuasa K. Type II cGMP-dependent protein kinase negatively regulates fibroblast growth factor signaling by phosphorylating Raf-1 at serine 43 in rat chondrosarcoma cells. *Biochem Biophys Res Commun* 2017;483:82–7.
- Ain NU, Iqbal M, Valta H, Emerling CA, Ahmed S, Makitie O, Naz S. Novel variants in natriuretic peptide receptor 2 in unrelated patients with acromesomelic dysplasia type Maroteaux. *Eur J Med Genet* 2019;62:103554.
- Bateman JF, Freddi S, Nattrass G, Savarirayan R. Tissue-specific RNA surveillance? Nonsense-mediated mRNA decay causes collagen X haploinsufficiency in Schmid metaphyseal chondrodysplasia cartilage. *Hum Mol Genet* 2003;12:217–25.
- Kemp BE, Pearson RB. Intracellular regulation of protein kinases and phosphatases. *Biochim Biophys Acta* 1991;1094:67–76.
- Vaandrager AB, Edixhoven M, Bot AG, Kroos MA, Jarchau T, Lohmann S, Genieser HG, de Jonge HR. Endogenous type II cGMP-dependent protein kinase exists as a dimer in membranes and can be functionally distinguished from the type I isoforms. *J Biol Chem* 1997;272:11816–23.
- Campbell JC, Kim JJ, Li KY, Huang GY, Reger AS, Matsuda S, Sankaran B, Link TM, Yuasa K, Ladbury JE, Casteel DE, Kim C. Structural basis of cyclic nucleotide selectivity in cGMP-dependent protein kinase II. *J Biol Chem* 2016;291:5623–33.
- Lohmann SM, Vaandrager AB, Smolenski A, Walter U, De Jonge HR. Distinct and specific functions of cGMP-dependent protein kinases. *Trends Biochem Sci* 1997;22:307–12.
- Raucci A, Laplantine E, Mansukhani A, Basilio C. Activation of the ERK1/2 and p38 mitogen-activated protein kinase pathways mediates fibroblast growth factor-induced growth arrest of chondrocytes. *J Biol Chem* 2004;279:1747–56.

- 28 Krejci P, Bryja V, Pachernik J, Hampl A, Pogue R, Mekikian P, Wilcox WR. FGF2 inhibits proliferation and alters the cartilage-like phenotype of RCS cells. *Exp Cell Res* 2004;297:152–64.
- 29 Chrisman TD, Garbers DL. Reciprocal antagonism coordinates C-type natriuretic peptide and mitogen-signaling pathways in fibroblasts. *J Biol Chem* 1999;274:4293–9.
- 30 Yasoda A, Komatsu Y, Chusho H, Miyazawa T, Ozasa A, Miura M, Kurihara T, Rogi T, Tanaka S, Suda M, Tamura N, Ogawa Y, Nakao K. Overexpression of CNP in chondrocytes rescues achondroplasia through a MAPK-dependent pathway. *Nat Med* 2004;10:80–6.
- 31 Tamura N, Doolittle LK, Hammer RE, Shelton JM, Richardson JA, Garbers DL. Critical roles of the guanylyl cyclase B receptor in endochondral ossification and development of female reproductive organs. *Proc Natl Acad Sci U S A* 2004;101:17300–5.
- 32 Vaandrager AB, Smolenski A, Tilly BC, Houtsmuller AB, Ehlert EM, Bot AG, Edixhoven M, Boomaars WE, Lohmann SM, de Jonge HR. Membrane targeting of cGMP-dependent protein kinase is required for cystic fibrosis transmembrane conductance regulator Cl⁻ channel activation. *Proc Natl Acad Sci U S A* 1998;95:1466–71.
- 33 Gambaryan S, Butt E, Marcus K, Glazova M, Palmethofer A, Guillon G, Smolenski A. cGMP-dependent protein kinase type II regulates basal level of aldosterone production by zona glomerulosa cells without increasing expression of the steroidogenic acute regulatory protein gene. *J Biol Chem* 2003;278:29640–8.
- 34 Spiessberger B, Bernhard D, Herrmann S, Feil S, Werner C, Luppa PB, Hofmann F. cGMP-dependent protein kinase II and aldosterone secretion. *Febs J* 2009;276:1007–13.
- 35 Mortier GR, Cohn DH, Cormier-Daire V, Hall C, Krakow D, Mundlos S, Nishimura G, Robertson S, Sangiorgi L, Savarirayan R, Sillence D, Superti-Furga A, Unger S, Warman ML. Nosology and classification of genetic skeletal disorders: 2019 revision. *Am J Med Genet A* 2019;179:2393–419.
- 36 Osebold WR, Remondini DJ, Lester EL, Spranger JW, Opitz JM. An autosomal dominant syndrome of short stature with mesomelic shortness of limbs, abnormal carpal and tarsal bones, hypoplastic middle phalanges, and bipartite calcanei. *Am J Med Genet* 1985;22:791–809.
- 37 Savarirayan R, Tofts L, Irving M, Wilcox W, Bacino CA, Hoover-Fong J, Ullot Font R, Harmatz P, Rutsch F, Bober MB, Polgreen LE, Ginebreda I, Mohnike K, Charrow J, Hoernschmeyer D, Ozono K, Alanay Y, Arundel P, Kagami S, Yasui N, White KK, Saal HM, Leiva-Gea A, Luna-González F, Mochizuki H, Basel D, Porco DM, Jayaram K, Fischeleva E, Huntsman-Labed A, Day J. Once-daily, subcutaneous vosoritide therapy in children with achondroplasia: a randomised, double-blind, phase 3, placebo-controlled, multicentre trial. *Lancet* 2020;396:684–92.
- 38 Breinholt VM, Rasmussen CE, Mygind PH, Kjølgaard-Hansen M, Faltinger F, Bernhard A, Zettler J, Hersel U, Holse Mygind P. TransCon CNP, a sustained-release C-type natriuretic peptide prodrug, a potentially safe and efficacious new therapeutic modality for the treatment of comorbidities associated with fibroblast growth factor receptor 3-related skeletal dysplasias. *J Pharmacol Exp Ther* 2019;370:459–71.
- 39 Garcia S, Dirat B, Tognacci T, Rochet N, Mouska X, Bonnafous S, Patouraux S, Tran A, Gual P, Le Marchand-Brustel Y, Gennero I, Gouze E. Postnatal soluble FGFR3 therapy rescues achondroplasia symptoms and restores bone growth in mice. *Sci Transl Med* 2013;5:203ra124.
- 40 Komla-Ebri D, Dambroise E, Kramer I, Benoist-Lassel C, Kaci N, Le Gall C, Martin L, Busca P, Barbault F, Gaus-Porta D, Munnich A, Kneissel M, Di Rocco F, Biosse-Duplan M, Legeai-Mallet L. Tyrosine kinase inhibitor NVP-BGJ398 functionally improves FGFR3-related dwarfism in mouse model. *J Clin Invest* 2016;126:1871–84.

Supplementary Information

Results of Exome sequencing

Proband 1: The average read depth was 145X. A total of 37346 variants were obtained for the proband. The variants were filtered (see methods). A recessive mode of inheritance was firstly considered due to the known consanguinity present in the family. A total of 13 homozygous variants were observed (Table S1).

Proband 2: The average read depth was 30X. A total of 33303 variants were obtained, 12308 of which altered the protein sequence, and 880 of these were rare variants with an allelic frequency of less than 0.1%. Further variant filtering was performed using in-house allelic frequency data, resulting in the total of 309 variants. Homozygous and compound heterozygous variants were firstly evaluated, with the presence of a total of seven homozygous variants (Table S2).

Supplemental Figure legends

Figure S1: Growth curve of the female proband from family 1. Height and weight data are indicated by black spots, bone age (red spot), adult target height (green spot and post-lengthening height (yellow spot). At age 12, she had advanced bone age (3 years) in relation to her chronological age. The growth curve is based on 2010 Spanish height data (<http://www.aeped.es/noticias/estudios-espanoles-crecimiento-2010>). The coloured lines represent the growth percentiles.

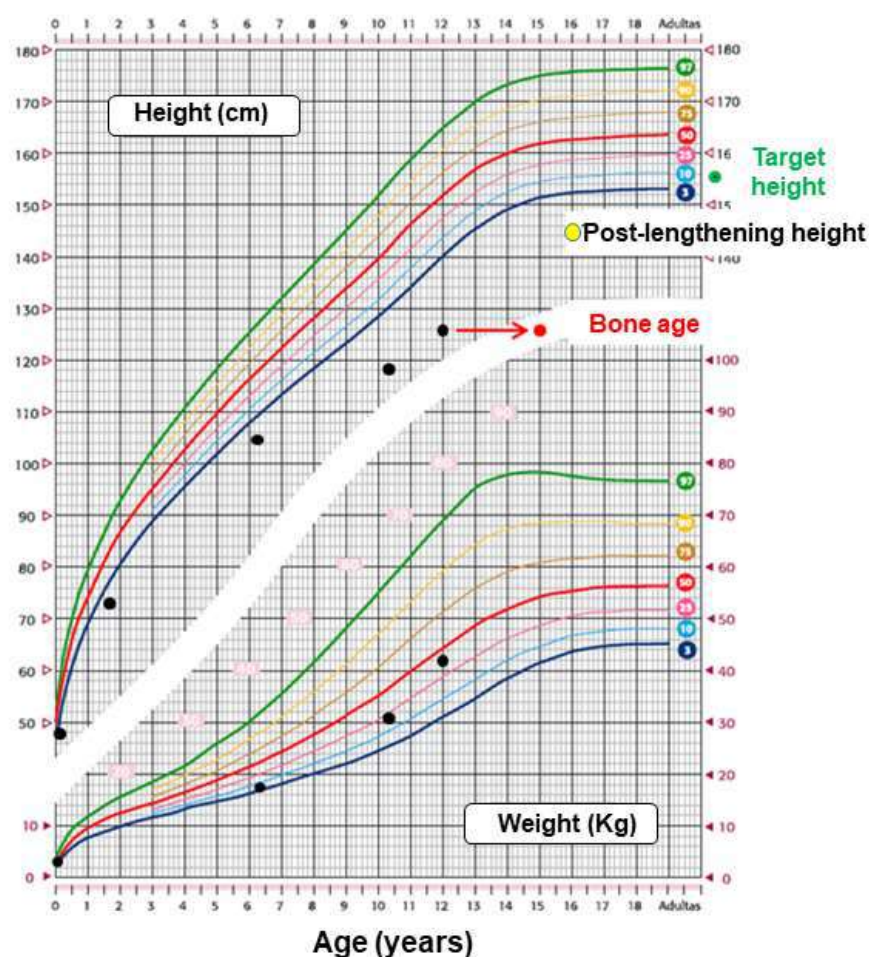


Figure S2: Evolution of skeletal anomalies of proband 2 at age 4, 7 and 11 years old.

Radiographs at 4 years (A, B, G, J, L, O), 7 years (C, D, H, M, P) and 11 years (E, F, I, K, N, Q). At age 4, moderate platyspondyly with anterior beaking of vertebral borders of dorso-lumbar spine was observed (A, B) which improved with age, at 7 years (C, D), and at 11 years (E, F). The ilia were short with flaring of the iliac wings (G, H, I at 4, 7, and 11 years old, respectively). At 7 years old, she had relatively large epiphyses and increased prominence of metaphyseal irregularity of long bones (P), which was not observed at age 4 (O) and that improved by age 11 (Q). Prominent deltoid tuberosities of the humeri were observed (J, K, at age 4 and 7 years respectively). She had short and broad phalanges and metaphyseal irregularity of metacarpals (L, M, N, at 4, 7, and 11 years old, respectively) and metatarsals (data not shown).

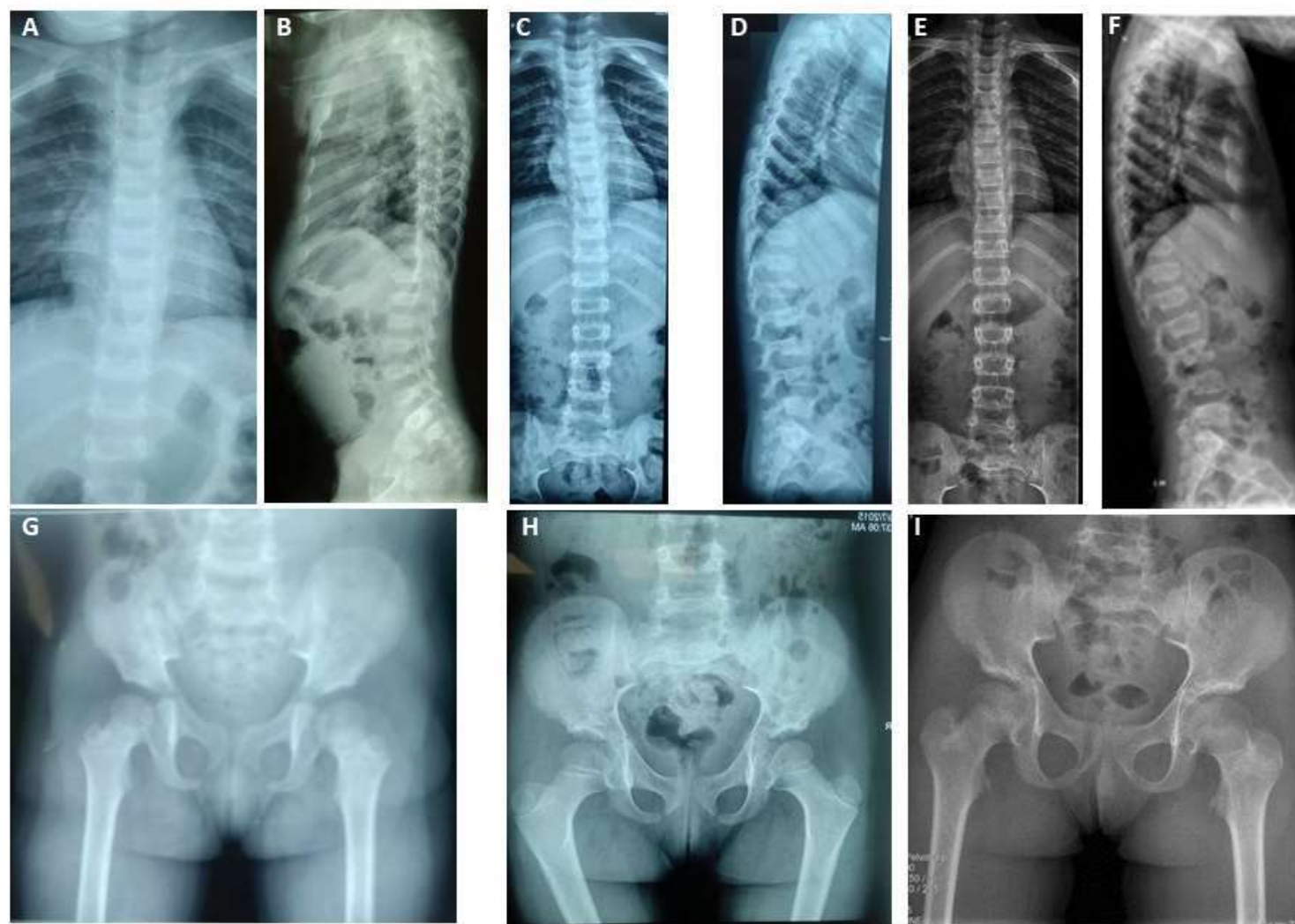
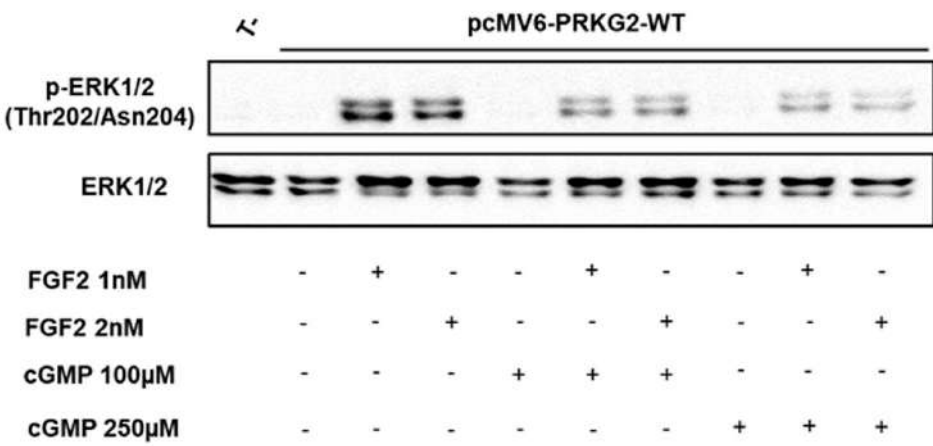




Fig S3: cGMP reduces FGF2 induced activation of p-ERK1/2 in HEK293T cells transfected with PRKG2-WT. Cells were treated with 100µM or 250µM cGMP for 30 minutes followed by the addition of 1nM or 2nM FGF2 for another 30 minutes. Cells were collected and lysed to obtain the protein. Western blot was subsequently performed for the determination of the activation/inhibition of ERK1/2 pathway as described in methods. FGF2 treatment activates ERK1/2 phosphorylation and the addition of cGMP dramatically reduces p-ERK1/2 independently of the concentration used.



Supplemental Tables

Table S1: Homozygous variants detected in the exome sequencing of proband 1.

| Chr. | Position (hg19) | Ref/Alt | Allelic depth | Gene | Variant cDNA and protein | Disorder [MIM] | Mode of inheritance |
|----------|-----------------|------------|---------------|---------------------------------------|--|---|---------------------|
| 1 | 32193790 | G/A | 0/189 | <i>ADGRB2</i> | NM_001294335.1:c.4505C>T; p.Thr1502Met | - | - |
| 1 | 33233498 | C/T | 1/231 | <i>KIAA1522</i> | NM_020888.2:c.346C>T; p.Pro116Ser | - | - |
| 1 | 45166717 | G/C | 0/94 | <i>C1orf228</i> | NM_001145636.1:c.565G>C; p.Gly189Arg | - | - |
| 1 | 55172208 | T/C | 0/107 | <i>MROH7</i> | NM_001039464.3:c.3665T>C; p.Ile1222Thr | Limb girdle muscular dystrophy [MIM 608807] | AR |
| 2 | 179393898 | T/A | 0/48 | <i>TTN</i> | NM_001267550.2:c.106580A>T; p.Glu35527Val | Salih myopathy [MIM 611705] | AR |
| 2 | 179398515 | C/T | 1/87 | <i>TTN</i> | NM_001267550.2:c.102827G>A; p.Arg34276Gln | Salih myopathy [MIM 611705] | AR |
| 2 | 179410721 | G/A | 0/199 | <i>TTN</i> | NM_001267550.2:c.95242C>T; p.Arg31748Cys | Salih myopathy [MIM 611705] | AR |
| 2 | 179448450 | G/A | 0/103 | <i>TTN</i> | NM_001267550.2:c.65459C>T; p.Thr21820Ile | Salih myopathy [MIM 611705] | AR |
| 2 | 179466171 | T/C | 0/132 | <i>TTN</i> | NM_001267550.2:c.55553A>G; p.Lys18518Arg | Salih myopathy [MIM 611705] | AR |
| 2 | 179486345 | T/A | 0/135 | <i>TTN</i> | NM_001267550.2:c.45206A>T; p.Glu15069Val | Salih myopathy [MIM 611705] | AR |
| 4 | 82056380 | G/A | 0/102 | <i>PRKG2</i> | NM_006259.2:c.1705C>T; p.Arg569* | - | - |
| 4 | 84390212 | C/A | 0/40 | <i>FAM175A</i> (<i>ABRAXAS1</i>) | NM_139076.2:c.569G>T; p.Gly190Val | - | - |
| 11 | 16824599 | C/T | 0/43 | <i>PLEKHA7</i> | NM_001329630.1:c.2077G>A; p.Val693Ile | - | - |

The pathogenic *PRKG2* variant is highlighted in bold. Chr. Chromosome; Ref: reference, Alt: variant; AR: autosomal recessive.

Table S2: Homozygous variants detected in the exome sequencing of proband 2.

| Chr. | Position (hg19) | Ref/Alt | Allelic depth | Gene | Variant cDNA and protein | Disorder [MIM] | Mode of inheritance |
|----------|-----------------|-------------|---------------|---------------------|---|---|---------------------|
| 4 | 69098125 | T/C | 1/15 | <i>TMPRSS11B</i> | NM_182502:c.479A>G; p.Lys160Arg | - | - |
| 4 | 82096083 | A/AT | 0/14 | <i>PRKG2</i> | NM_006259:c.491dupA; p.Asn164Lysfs*2 | - | - |
| 4 | 1.06E+08 | A/G | 0/6 | <i>TET2</i> | NM_001127208:c.3583A>G; p.Ile1195Val | Myelodysplastic syndrome, somatic [MIM 614286] | Somatic |
| 4 | 1.4E+08 | T/A | 0/8 | <i>SETD7</i> | NM_001306199:c.898A>T; p.Thr300Ser | - | - |
| 4 | 1.48E+08 | C/T | 0/9 | <i>POU4F2</i> | NM_004575:c.1028C>T; p.Ala343Val | - | - |
| 22 | 50664251 | C/T | 0/13 | <i>TUBGCP6</i> | NM_020461:c.1955G>A; p.Arg652His | Microcephaly and chorioretinopathy, autosomal recessive, 1 [MIM 251270] | AR |
| 22 | 50905771 | G/A | 0/17 | <i>SBF1</i> | NM_002972:c.545C>T; p.Ser182Leu | Charcot-Marie-Tooth disease, type 4B3 [MIM 615284] | AR |

All variants are Quality filtered passed and Phred-scaled likelihoods (PL) values of 0 for the called genotype. The pathogenic *PRKG2* variant is highlighted in bold. Chr. Chromosome; Ref: reference, Alt: variant; AR: autosomal recessive.

Supplementary Information

Results of Exome sequencing

Proband 1: The average read depth was 145X. A total of 37346 variants were obtained for the proband. The variants were filtered (see methods). A recessive mode of inheritance was firstly considered due to the known consanguinity present in the family. A total of 13 homozygous variants were observed (Table S1).

Proband 2: The average read depth was 30X. A total of 33303 variants were obtained, 12308 of which altered the protein sequence, and 880 of these were rare variants with an allelic frequency of less than 0.1%. Further variant filtering was performed using in-house allelic frequency data, resulting in the total of 309 variants. Homozygous and compound heterozygous variants were firstly evaluated, with the presence of a total of seven homozygous variants (Table S2).

Supplemental Figure legends

Figure S1: Growth curve of the female proband from family 1. Height and weight data are indicated by black spots, bone age (red spot), adult target height (green spot and post-lengthening height (yellow spot). At age 12, she had advanced bone age (3 years) in relation to her chronological age. The growth curve is based on 2010 Spanish height data (<http://www.aeped.es/noticias/estudios-espanoles-crecimiento-2010>). The coloured lines represent the growth percentiles.

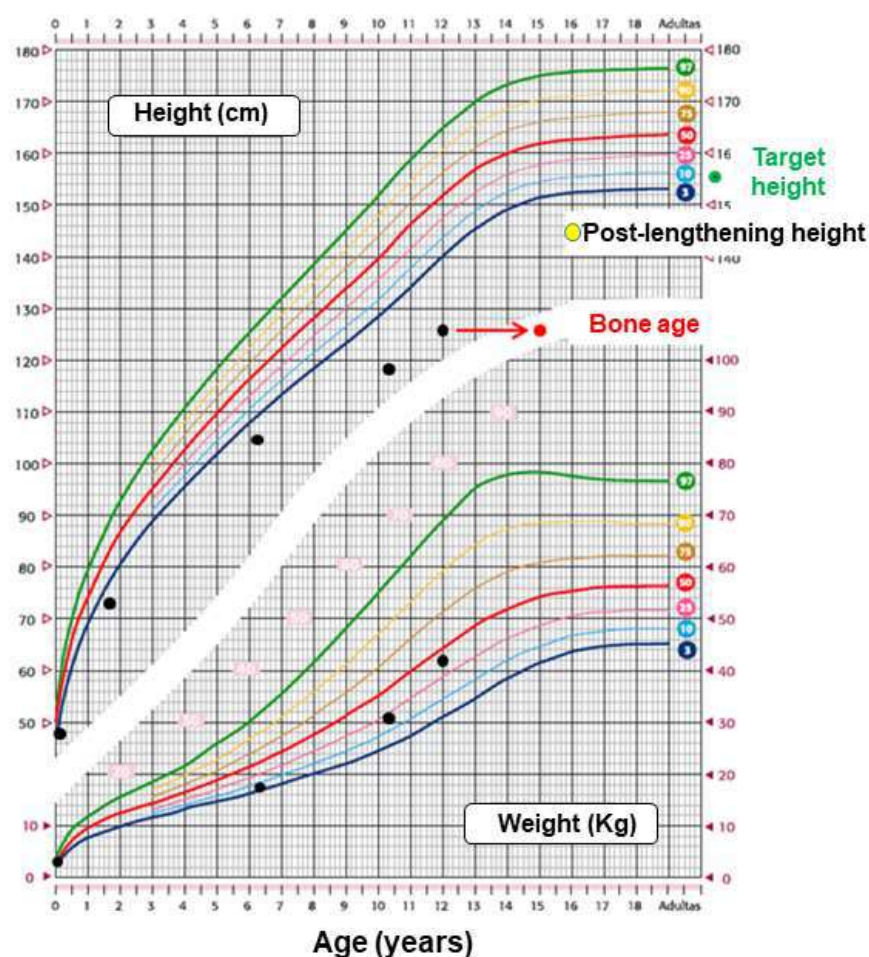


Figure S2: Evolution of skeletal anomalies of proband 2 at age 4, 7 and 11 years old.

Radiographs at 4 years (A, B, G, J, L, O), 7 years (C, D, H, M, P) and 11 years (E, F, I, K, N, Q). At age 4, moderate platyspondyly with anterior beaking of vertebral borders of dorso-lumbar spine was observed (A, B) which improved with age, at 7 years (C, D), and at 11 years (E, F). The ilia were short with flaring of the iliac wings (G, H, I at 4, 7, and 11 years old, respectively). At 7 years old, she had relatively large epiphyses and increased prominence of metaphyseal irregularity of long bones (P), which was not observed at age 4 (O) and that improved by age 11 (Q). Prominent deltoid tuberosities of the humeri were observed (J, K, at age 4 and 7 years respectively). She had short and broad phalanges and metaphyseal irregularity of metacarpals (L, M, N, at 4, 7, and 11 years old, respectively) and metatarsals (data not shown).

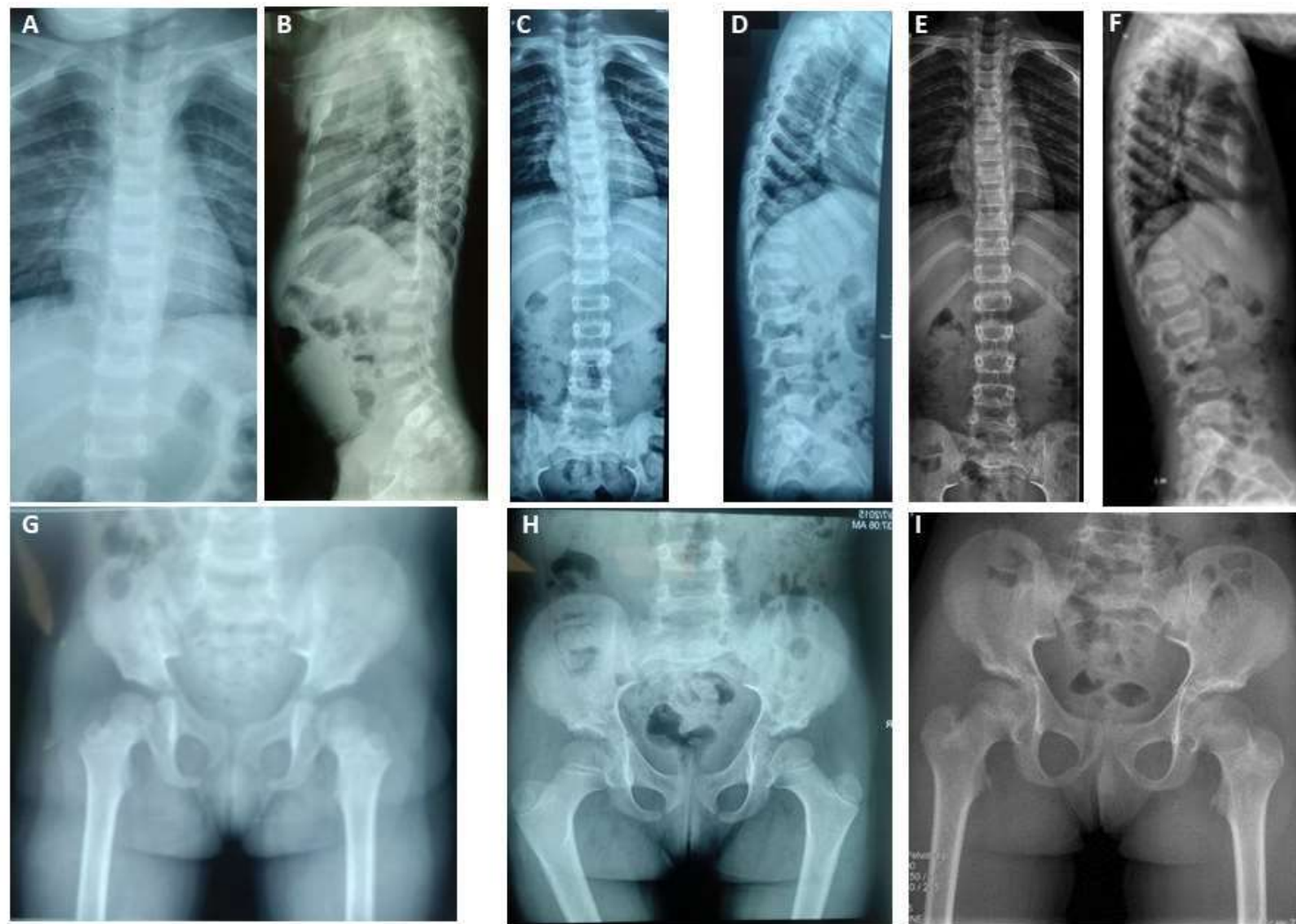
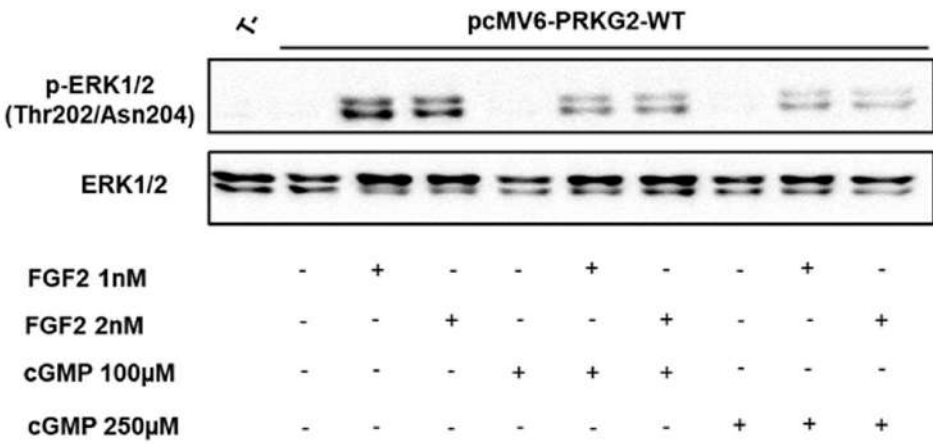




Fig S3: cGMP reduces FGF2 induced activation of p-ERK1/2 in HEK293T cells transfected with PRKG2-WT. Cells were treated with 100µM or 250µM cGMP for 30 minutes followed by the addition of 1nM or 2nM FGF2 for another 30 minutes. Cells were collected and lysed to obtain the protein. Western blot was subsequently performed for the determination of the activation/inhibition of ERK1/2 pathway as described in methods. FGF2 treatment activates ERK1/2 phosphorylation and the addition of cGMP dramatically reduces p-ERK1/2 independently of the concentration used.



Supplemental Tables

Table S1: Homozygous variants detected in the exome sequencing of proband 1.

| Chr. | Position (hg19) | Ref/Alt | Allelic depth | Gene | Variant cDNA and protein | Disorder [MIM] | Mode of inheritance |
|----------|-----------------|------------|---------------|---------------------------------------|--|---|---------------------|
| 1 | 32193790 | G/A | 0/189 | <i>ADGRB2</i> | NM_001294335.1:c.4505C>T; p.Thr1502Met | - | - |
| 1 | 33233498 | C/T | 1/231 | <i>KIAA1522</i> | NM_020888.2:c.346C>T; p.Pro116Ser | - | - |
| 1 | 45166717 | G/C | 0/94 | <i>C1orf228</i> | NM_001145636.1:c.565G>C; p.Gly189Arg | - | - |
| 1 | 55172208 | T/C | 0/107 | <i>MROH7</i> | NM_001039464.3:c.3665T>C; p.Ile1222Thr | Limb girdle muscular dystrophy [MIM 608807] | AR |
| 2 | 179393898 | T/A | 0/48 | <i>TTN</i> | NM_001267550.2:c.106580A>T; p.Glu35527Val | Salih myopathy [MIM 611705] | AR |
| 2 | 179398515 | C/T | 1/87 | <i>TTN</i> | NM_001267550.2:c.102827G>A; p.Arg34276Gln | Salih myopathy [MIM 611705] | AR |
| 2 | 179410721 | G/A | 0/199 | <i>TTN</i> | NM_001267550.2:c.95242C>T; p.Arg31748Cys | Salih myopathy [MIM 611705] | AR |
| 2 | 179448450 | G/A | 0/103 | <i>TTN</i> | NM_001267550.2:c.65459C>T; p.Thr21820Ile | Salih myopathy [MIM 611705] | AR |
| 2 | 179466171 | T/C | 0/132 | <i>TTN</i> | NM_001267550.2:c.55553A>G; p.Lys18518Arg | Salih myopathy [MIM 611705] | AR |
| 2 | 179486345 | T/A | 0/135 | <i>TTN</i> | NM_001267550.2:c.45206A>T; p.Glu15069Val | Salih myopathy [MIM 611705] | AR |
| 4 | 82056380 | G/A | 0/102 | <i>PRKG2</i> | NM_006259.2:c.1705C>T; p.Arg569* | - | - |
| 4 | 84390212 | C/A | 0/40 | <i>FAM175A</i> (<i>ABRAXAS1</i>) | NM_139076.2:c.569G>T; p.Gly190Val | - | - |
| 11 | 16824599 | C/T | 0/43 | <i>PLEKHA7</i> | NM_001329630.1:c.2077G>A; p.Val693Ile | - | - |

The pathogenic *PRKG2* variant is highlighted in bold. Chr. Chromosome; Ref: reference, Alt: variant; AR: autosomal recessive.

Table S2: Homozygous variants detected in the exome sequencing of proband 2.

| Chr. | Position (hg19) | Ref/Alt | Allelic depth | Gene | Variant cDNA and protein | Disorder [MIM] | Mode of inheritance |
|----------|-----------------|-------------|---------------|---------------------|---|---|---------------------|
| 4 | 69098125 | T/C | 1/15 | <i>TMPRSS11B</i> | NM_182502:c.479A>G; p.Lys160Arg | - | - |
| 4 | 82096083 | A/AT | 0/14 | <i>PRKG2</i> | NM_006259:c.491dupA; p.Asn164Lysfs*2 | - | - |
| 4 | 1.06E+08 | A/G | 0/6 | <i>TET2</i> | NM_001127208:c.3583A>G; p.Ile1195Val | Myelodysplastic syndrome, somatic [MIM 614286] | Somatic |
| 4 | 1.4E+08 | T/A | 0/8 | <i>SETD7</i> | NM_001306199:c.898A>T; p.Thr300Ser | - | - |
| 4 | 1.48E+08 | C/T | 0/9 | <i>POU4F2</i> | NM_004575:c.1028C>T; p.Ala343Val | - | - |
| 22 | 50664251 | C/T | 0/13 | <i>TUBGCP6</i> | NM_020461:c.1955G>A; p.Arg652His | Microcephaly and chorioretinopathy, autosomal recessive, 1 [MIM 251270] | AR |
| 22 | 50905771 | G/A | 0/17 | <i>SBF1</i> | NM_002972:c.545C>T; p.Ser182Leu | Charcot-Marie-Tooth disease, type 4B3 [MIM 615284] | AR |

All variants are Quality filtered passed and Phred-scaled likelihoods (PL) values of 0 for the called genotype. The pathogenic *PRKG2* variant is highlighted in bold. Chr. Chromosome; Ref: reference, Alt: variant; AR: autosomal recessive.